SURFACE FORCES OF COLLOIDAL PARTICLES FROM MICROMETER TO NANOMETER

By

JEONG-MIN CHO

A DISSERTATION PRESENTED TO THE GRADUATE SCHOOL
OF THE UNIVERSITY OF FLORIDA IN PARTIAL FULFILLMENT
OF THE REQUIREMENTS FOR THE DEGREE OF
DOCTOR OF PHILOSOPHY

UNIVERSITY OF FLORIDA

2003

Copyright 2003

by

Jeong-Min Cho

This dissertation is dedicated to my parents; and to my wife, Eunkyung.

ACKNOWLEDGMENTS

I would like to acknowledge my advisor, Dr. Wolfgang M. Sigmund, for giving me the opportunity to improve my scientific knowledge and professional research skills. Many of the achievements during my Ph. D. career would not have been possible without his excellent guidance and support.

Dr. Brij M. Moudgil, Dr. Dinesh O. Shah, Dr. Susan B. Sinnott, Dr. Laurie B. Gower, and Dr. Abbas Zaman, are appreciated for serving as my advisory committee. I would also like to thank the National Science Foundation's Particle Engineering Research Center (PERC) and industrial partners for financially supporting this research.

My graduate school years were made more productive by collaboration with past and present graduate students in our research group and PERC including Joshua Adler, Georgios Pygiotakis, Vasana Maneeratana, Seungwoo Lee, Kihong Lee, Hansoo Kim, Madhavan Esayanur, Wonseop Choi, Seungmahn Lee, Jungsik Bang, Joodong Park, Yiyeon Kim, Dongsik Kim, Sanhyun Yoon, Wonseok Kim, Bumsu Kim, Hyun Cho, Navin Manjooran, and all of the other friends who made my last 4 years valuable and delightful.

Lastly, I would like to express a deep appreciation to my parents and family. I especially thank my wife, Eunkyung Lee, for trusting and supporting me throughout my study; and for giving birth to my lovely daughter, Heejin.

TABLE OF CONTENTS

Page

ACKNOWLEDGMENTS iv

LIST OF TABLES viii

LIST OF FIGURES ix

ABSTRACT xii

CHAPTER

1 INTRODUCTION 1

2 FORCE THEORY 5

van der Waals Force 5
Microscopic Approach 7
Macroscopic Approach 8
Retardation and Screening 11
Geometry: The Derjaguin Approximation 12
Electric Double Layer Force 14
Charging of Surfaces 14
Point of Zero Charge (PZC) 15
Electric Double Layer (EDL) 16
Zeta Potential 20
EDL Interaction between Charged Surfaces 22
Boundary Conditions for Calculating EDL Forces 23
DLVO Theory 25
Steric Force 28
Polymers in Solution 29
Excluded Volume 30
Polyelectrolytes in Solution 31
Polymer Layers on a Surface 32
Interaction between Polymer Coated Surfaces 34
Surface Force Measurement Techniques 35
Conversion of Raw Data to Force-Separation Curves 37
Determination of Spring Constant 39
Summary 41

3 ADSORPTION OF POLYETHYLENEIMINE (PEI) ON SILICA PARTICLES AND DISPERSION BEHAVIOR....42

Introduction....42
Experimental....44
Materials....44
Methods....45
Results....46
Adsorption of PEI....47
Turbidity....51
Discussion....55
Effect of pH....55
Effect of Ionic Strength....57
Effect of Molecular Weight....58
Summary....63

4 SURFACE FORCES BETWEEN PEI LAYERS ADSORBED TO SILICA SURFACES....65

Introduction....65
Experimental....67
Materials....67
Method....68
Results and Discussion....69
Interaction Forces between Bare Silica Surfaces....69
Interaction Forces between PEI Layers Adsorbed to Silica Microsphere and Substrate....74
Interaction Forces between PEI Layers Adsorbed to Si tip and Silica Substrate 81
Summary....85

5 SURFACE FORCE MEASUREMENT USING NANO COLLOIDAL PROBE TECHNIQUE....87

Introduction....87
Experimental....89
Materials....89
Preparation of Nanotube-Attached AFM Tip....90
Force Measurement....92
Results and Discussion....92
Theoretical Calculation for the Effect of Tip Geometry....92
Surface force between Nanotube Tip and Substrate....95
Summary....101

6 EFFECT OF PARTICLE SIZE IN POLYMERIC FORCES....103

Introduction....103
Experimental....104

Results and Discussion 105
Effect of the Colloidal Probe Size 107
Fitting the Interaction Force of MWNT Tip 112
Effect of Non-adsorbed Free Polymer 114
Summary 118

7 CONCLUSION 119

LIST OF REFERENCES 122

BIOGRAPHICAL SKETCH 129

LIST OF TABLES

Table page

2-1 Nonretarded vdW attraction energy and force between different geometries.....7

2-2 Solution to the PB equation for high and low surface potentials 20

4-1 Calculated Flory radius, R_F and radius of gyration, R_g for different Mw PEIs.....67

6-1 The fitting equation for the interaction force of MWNT tip 113

LIST OF FIGURES

Figure page

2-1 Normalized vdW forces between a sphere and a plate as a function of separation.....13

2-2 The electric double layer (EDL) model developed on the charged surface. 19

2-3 Potential profile versus separation between two opposing electric double layers. 22

2-4 The calculated total interaction energy.....27

2-5 Typical polymer structures on the surface.....33

2-6 Standard colloidal probe technique for measuring directly interaction force between surfaces in the liquid cell mode of the AFM. 36

2-7 Surface forces measured with an AFM colloidal probe technique.....38

3-1 Structure of polyethyleneimine (PEI).....44

3-2 Zeta potential of silica particles with or without PEI 47

3-3 Adsorption isotherm for PEI (Mw=10,000) on SiO_2 as a function of pH in $5x10^{-4}$ M NaCl solution.....48

3-4 Adsorption isotherm for PEI (Mw=10,000) on SiO_2 as a function of pH in NaCl solution (a) $3x10^{-3}$ M, (b) 10^{-2} M. 49

3-5 Adsorption isotherm for PEI (Mw=600) on SiO_2 in $5x10^{-4}$ M NaCl.....50

3-6 Adsorption isotherm for PEI (Mw=1,800) on SiO_2 in $5x10^{-4}$ M NaCl.....51

3-7 Change of turbidity of silica suspension measured at pH 10 and 0.0005 M NaCl (a) with varying the concentration of PEI 600 as a function of time.....52

3-8 Change of turbidity of silica suspension measured at pH 10 and 0.0005 M NaCl (a) with varying the concentration of PEI 1,800 as a function of time.....53

3-9 Change of turbidity of silica suspension measured at pH 10 and 0.0005 M NaCl (a) with varying the concentration of PEI 10,000 as a function of time.....54

3-10 The amount of maximum adsorption of PEI (Mw=10,000) on SiO_2 powder 59

3-11 A logarithmic plot of maximum adsorption of PEI (Γ_{max}) on SiO_2.....60

3-12 Adsorption isotherm and turbidity of SiO_2 suspension with PEI 600 61

3-13 Adsorption isotherm and turbidity of SiO_2 suspension with PEI 10,000 63

4-1 Materials used for surface force measurement. 69

4-2 Normalized force-separation profile plot between silica probe and silica substrate in $4x10^{-4}$ M NaCl solution.....71

4-3 Normalized force-separation profile between silica probe and silica substrate with varing NaCl concentration at pH 10.....73

4-4 Interaction forces between silica surfaces with different amount of PEI (Mw=1,800) at pH 10 in pure water 75

4-5 Normalized force-separation profile between silica probe and silica substrate with PEI 600 at different pH in $5x10^{-4}$ M NaCl concentration. 76

4-6 Normalized interaction forces between silica sphere and silica plate surface with adsorption in 2,000 mg/L of PEI solution (Mw=10,000) at pH 4 and 10 in $3x10^{-3}$ M NaCl. 77

4-7 Normalized interaction forces between silica sphere and silica plate surface with adsorption in 2,000 mg/L of PEI solution (Mw=10,000) at pH 4 as a function of ionic strength 78

4-8 Normalized interaction forces between silica sphere and silica plate surface with adsorption in 2,000 mg/L of PEI solution (Mw=1,800) at pH 10 as a function of ionic strength. 79

4-9 A proposed model of different conformation of PEI adsorbed on silica surfaces with varying pH and ionic strength. 81

4-10 Force-separation profile between Si tip and silica substrate with PEI 1,800 at different pH and NaCl concentration. 82

4-11 Force-separation profile between Si tip and silica substrate with different molecular weight PEI at pH 10 in $5x10^{-4}$ M NaCl concentration 83

4-12 Force-separation profile between Si tip and silica substrate with PEI 10,000 at different pH in $5x10^{-4}$ M NaCl concentration. 84

5-1 Preparation of the MWNT tip using a micromanipulator under the optical microscope. 91

5-2 Calculated van der Waals interaction force between a cone shaped AFM tip and a flat plate depending on the angle θ. 93

5-3 The calculated van der Waals interaction force between the colloidal probe and flat plate depending on the tip geometry. 94

5-4 FESEM image of a MWNT bundle attached to the AFM tip....95

5-5 Deflection-displacement between highly oriented pyrolytic graphite (HOPG) and MWNT probe at different pH....96

5-6 Force-separation profile between MWNT tip and HOPG substrate....98

5-7 Interaction forces between MWNT tip and silica substrate as a function of ionic strength at pH 4. 100

5-8 Interaction forces between MWNT tip and silica substrate as a function of ionic strength at pH 10 101

6-1 Interaction force between MWNT tip and silica substrate with a different concentration of PEI 10,000 in 0.01 M NaCl at pH 10....106

6-2 Force vs. separation plot between a glassy carbon and SiO_2 substrate in PEI 70,000 solution....108

6-3 Force vs. separation plot between a MWNT probe and SiO_2 substrate. 109

6-4 Force vs. separation plot between a bare Si tip and SiO_2 substrate....110

6-5 Interaction force between MWNT tip and silica substrate with 2000 mg/L PEI of different molecular weight in 0.01 M NaCl at pH 10. 111

6-6 Force-separation profile of nanotube tip in presence of PEI 70,000. 113

6-7 Interaction force between silica sphere and silica substrate at pH 10, 0.0001M as a function of concentration of colloidal silica....115

6-8 Force versus separation plot between a glassy carbon probe and SiO_2 substrate before and after washing out the non-adsorbed polymer in the solution....116

6-9 Force versus separation plot between a MWNT tip and SiO_2 substrate before and after washing out the non-adsorbed polymer in the solution. 117

Abstract of Dissertation Presented to the Graduate School
of the University of Florida in Partial Fulfillment of the
Requirements for the Degree of Doctor of Philosophy

SURFACE FORCES OF COLLOIDAL PARTICLES FROM MICROMETER TO NANOMETER

By

Jeong-Min Cho

December 2003

Chair: Wolfgang M. Sigmund
Major Department: Materials Science and Engineering

Surface forces of colloidal particles play critical roles in the macroscopic behavior of particulate systems such as dispersion and coagulation, adhesion and coating, and the rheological behavior of ceramic slurries. As particle size is decreased from micrometer to nanometer range, surface forces are increasingly important. Polyelectrolytes are the chemical additives commonly used to efficiently control the stabilization of the colloidal system. Their conformations on the solid surfaces as well as the interactions between the adsorbed polyelectrolytes are important issues in colloidal processing. Most experimental and theoretical approaches to the surface forces are based on particle sizes in the micrometer range. However, nanoparticles at close proximity or high solids loading are expected to show different behavior than what can be estimated from conventional theories such as continuum or mean field theories.

My study examined the effect of pH, ionic strength, and molecular weight of the polyelectrolytes on the surface forces of colloidal particles by the interplay with the adsorption, turbidity, and direct surface force measurement in terms of the conformation

on the solid surfaces. The colloid probe technique based on atomic force microscopy (AFM) is well established for micron size particles; and could be extended for nanosize particles by using carbon nanotubes as proximal probes. Nanotubes with their high aspect ratio avoid the contribution from cone shapes that happens with AFM tips. The difference in particle size significantly influences surface forces for sterically dispersed colloidal systems.

CHAPTER 1
INTRODUCTION

The term "colloids" is widely defined as particles or domains with sizes in the range of 1 to 1000 nm. The fundamental characteristics of interaction between colloidal particles are mainly surface-related phenomena because of their larger specific surface area, up to several hundred meters per gram. Interaction between the colloids plays a considerable role in many particulate systems, for instance, powder flow, ink and paint pigments, adhesion, coating, chemical mechanical planarization (CMP) slurry, and biological application. When two or more colloidal particles are interacting, their movements are affected by several types of interaction such as gravitational force, Brownian motion, and surface forces.

Surface forces between two interacting bodies have been studied for several decades. They are known to originate from the interatomic forces acting among all of the atoms of those bodies, as well as the atoms of any intervening medium. Aside from this simple interpretation, there are several discrete surface forces acting between colloids which can be classified as van der Waals force, electric double layer force, hydration force, hydrophobic force, and steric force, details of which will be described in Chapter 2. The behavior and properties of the colloidal system, such as dispersion and agglomeration of the particulates and viscosity of the slurries, are determined by the net balance of all of these forces since there is competition among surface forces and some particular dominant mechanisms decide the total forces. Hence, it is important to

understand the fundamentals of surface forces in controlling the stability of colloidal systems.

Theoretical and experimental approaches for investigating surface forces have widely been developed for particles in the millimeter to micrometer size range. However, the scalability of those theories down to the nanometer size range is questionable because premises required to develop the current theories directly exclude the nanometer range. For instance, the Derjarguin approximation, which translates from the interaction energy between two flat surfaces into other shapes, like sphere-sphere and sphere-plane, is only valid when the radius of the particle is much greater than the separation distance between two particles. The Poisson-Boltzmann equation is based on point charges, which cannot be considered for a very short separation distance or for small particles, since the contribution to the increase of effective volume by ion size is not negligible for very small particles. Therefore, the fundamental understanding and more precise control of the surface chemistry of the nanometer-sized colloidal particles is especially important as modern technologies demand great performance with smaller-dimension products.

Chemical additives such as surfactants, polymers, or polyelectrolytes are normally used to efficiently manipulate the stability of the colloidal system. The presence of these chemical additives can change the interaction behavior of colloidal particles; and the basic stabilization mechanism is induced by the interaction of the polymer molecular chains. The polymer-induced surface forces are affected by the nature of the polymer (i.e., structure of polymer, ionizability, conformation on surfaces) and the physicochemical condition of the system (i.e., solvent quality, pH, ionic strength). Not just these parameters but also the relative size of polymer molecules and particles must be

considered for the nanoparticles. The different conformation of a polymer is expected because of the large curvature of small particles; and a significant increase in the effective volume of particles may induce dramatic change in the macroscopic colloidal behavior of the nanoparticulate system. In addition, exemplary theories such as scaling or mean field theory describing interactions between polymer layers are also not valid for nanoparticles because of failure of continuum approach to this regime.

Besides the above-mentioned theoretical limits, there is also an experimental challenge to directly measure surface forces of nanoparticles. Although several techniques such as surface force apparatus (SFA) and atomic force microscopy (AFM) colloidal probe technique have been employed for several decades, these techniques can measure interaction forces of relatively large samples, which are bigger than the size limit of Derjaguin approximation. There is few force measurement technique being capable of directly measuring the surface forces of nanoparticles.

The objective of the studies in this dissertation is first to study the interaction of polyelectrolyte-adsorbed surfaces as a function of several controlling parameters (i.e., pH, ionic strength and molecular weight) by investigating the adsorption and turbidity and comparing them with surface force measurements. The second objective is to demonstrate the technique to directly measure the interaction force of nanometer-sized particles and improve the knowledge concerning the effect of particle size on surface forces in presence of polyelectrolytes.

The dissertation is organized as follows: existing theories of surface forces and force measurement technique is described in Chapter 2. Chapter 3 discusses the adsorption of polyelectrolyte and dispersion behavior, which are correlated to surface

force measurements in Chapter 4. In Chapter 5, a modified colloidal probe technique to measure surface forces of nanoparticles is introduced and compared with the conventional colloidal probe technique. Chapter 6 discusses some force measurements, which are dependent on the size of the colloidal probe, in the presence of polymer. Finally, Chapter 7 offers conclusions.

CHAPTER 2
FORCE THEORY

Surface forces are often used with the term "interface force" between two different materials or phases. With the development of the quantum theory, it was established that all surface forces are electrostatic and electrodynamic in origin. Surface forces are normally classified as some categories such as short-range and long-range forces. For example, electric double layer force is considered a long-range force and van der Waals force is considered a short-range force on a macroscopic scale but a long-range on an atomic scale. This chapter covers surface forces on a macroscopic scale.

van der Waals Force

In 1897, the Dutch scientist van der Waals [1] modified a conventional ideal gas law, PV=nRT, to

$$\left(P+\frac{n^2a}{V}\right)(V-nb)=nRT \tag{2-1}$$

where P is pressure, n is the number of moles of gas, V is the volume, R is the gas constant, T is temperature, and a and b are constant specific to a particular gas, by considering the occupied volume of the molecules and assuming attractive interactions between the molecules. Since then, the various types of attractive forces between the molecules are generally termed *van der Waals forces*. van der Waals (vdW) forces are always present between all molecules and attractive for symmetric systems. Thus, the condensations of the materials, which are electrically neutral and chemically saturated, have been explained by vdW forces. Sometimes a repulsive interaction can be observed

only for asymmetric systems due to a negative Hamaker constant [2, 3]. The Hamaker constant can be obtained from the optical properties of the interacting bodies and medium between them. The vdW force is a practically important force in nearly all areas of science, for examples, the wetting of solids by liquids, capillarity of liquids, adhesion of materials, structure of biological cell walls, and aggregation of the colloidal suspensions in the absence of repulsive forces.

The vdW force arises from the interaction between atomic and/or molecular dipoles. Those dipoles may exist by the structure of the molecule; or they may be transient or be induced by the molecule-molecule interaction. According to the origin of the dipoles, they are classified in three main categories.

- **Keesom interaction** The dipoles are permanent and are created by the structure of the molecule, like water. The dipole creates a finite electric field and this field can orient the neighbor dipoles so they are attracted to the first one [4, 5].
- **Debye interaction** A permanent dipole can induce a dipole in a polarizable atom or molecule. The new induced dipole is oriented again in a way that it is attracted to the first one [6].
- **London or dispersion interaction** The fluctuation of the electron distribution around the nucleus induces dipoles among the surroundings atoms or molecules and those induced dipoles are attracted to each other [7].

Keesom and Debye interaction forces cannot explain the universal vdW forces because these forces require the presence of permanent dipoles. London introduced the idea of interaction between two polarizable atoms or molecules. The attractive London dispersion forces between two atoms at distance, r, can be described as

$$W_{atom/atom} = -\frac{C}{r^6} \tag{2-2}$$

The London dispersion force constant, C, is related to the polarizability of the molecules.

Microscopic Approach

One way to calculate the vdW force is the Hamaker approximation, which is based on a pair-wise summation over all the atoms in the interacting bodies. Hamaker [8] showed that the nonretarded vdW interaction energy of two spheres with radius a is dependent on the center-center distance r as

$$W_{vdW}(r) = -\frac{A}{6}\left[\frac{2a^2}{r^2-4a^2} + 2\frac{a^2}{r^2} + \ln\left(1-2\frac{a^2}{r^2}\right)\right] \tag{2-3}$$

and if $a >> r$, this energy can be expressed simply with the separation distance D

$$F(D) = -\frac{AR_s}{12D^2}, \left(A=\pi^2 C\rho_1\rho_2\right) \tag{2-4}$$

Table 2-1. Nonretarded vdW attraction energy and force between different geometries calculated on the basis of pairwise additivity (Hamaker summation method) where A is the Hamaker constant, D is surface separation distance, and R_1 and R_2 are the radii of particle/cylinder.

Geometry of Interaction	Energy of Interaction (J)	Force of Interaction (N)
Plate/Plate	$-\frac{A}{12\pi D^2}$	$\frac{A}{6\pi D^3}$
Sphere/Plate	$-\frac{AR}{6D}$	$\frac{AR}{6D^2}$
Sphere/Sphere	$-\frac{A}{6D}\frac{R_1R_2}{(R_1+R_2)}$	$\frac{A}{6D^2}\frac{R_1R_2}{(R_1+R_2)}$
Crossed Cylinders	$-\frac{A\sqrt{R_1R_2}}{6D}$	$\frac{A\sqrt{R_1R_2}}{6D^2}$

where A is the Hamaker constant and depends on the polarizability and the number of atoms per unit volume in the two interacting bodies (ρ), and R_S is the radius of the sphere. de Boer [9] also calculated the vdW interaction for parallel plane solids and vdW forces of the various geometries of interacting bodies were summarized in Table 2-1.

Macroscopic Approach

Because of the many body effects, by which an electric field of one given atom is induced by not only the closest atom but also the atoms in the vicinity, Lifshitz proposed considering the bodies as a continuum with certain dielectric properties [10]. In addition, although vdW forces are mainly dominated by London dispersion forces induced from the interaction between instantaneous dipoles, there are many fundamental interactions contributing to the total interaction force such as charge/charge, charge/dipole, hydrogen bonding, etc. [11]. In real systems, intervening media atoms also have a significant impact on the interactions. Thus, a new approach other than the Hamaker method is required to account for these interactions of all types of species in a material. The advantage of the Lifshitz theory is that accurate prediction of the vdW force is possible if complete optical data is available. The fundamental of this approach is that absorption of an electromagnetic energy is affected by the static and oscillatory fields of the atomic elements in the material, resulting in differences in the dielectric spectra. However, it is difficult to measure the entire dielectric function over the wide range of frequencies although spectral optical properties over very wide energy ranges can be obtained from optical reflectivity [12], valence electron energy loss spectroscopy (VEELS) [13], or band structure calculations [14].

The accuracy of the optical properties is critical to the accuracy of the calculated Hamaker constant but simple spectral models or index approximations can be used where extensive data are not available. The simple spectral method was proposed by Ninham and co-workers [15, 16]. They used a set of parametric damped Lorentz oscillators, corresponding to absorptions at certain frequencies, which are the regions of dielectric relaxation. These resonant vibrations can be fitted to the physical properties such as absorption spectra, refractive index, or dielectric constant. This relation can be expressed as

$$\varepsilon(i\xi) = 1 + \sum_{i=1}^{N} \frac{C_i}{1 + \left(\frac{\xi}{\omega_i}\right)^2} \tag{2-5}$$

where ε is the dielectric constant as a function of the imaginary frequency iξ, spectral constant, $C_i=(2/\pi)(f_i/\omega_i)$ and f_i is the strength of the oscillator at characteristic absorption frequency ω_i, and ξ is a constant frequency equal to $(4\pi^2 kT/h)$ in which k is Boltzmann's constant, T is absolute temperature, and h is Plank's constant. C_i and ω_i can be calculated from the Cauchy equation (2-6) and relation (2-7). For example, for a UV oscillator,

$$n^2(\omega) - 1 = \left(n^2(\omega) - 1\right)\frac{\omega^2}{\omega_{UV}^2} + C_{UV} \tag{2-6}$$

$$C_{UV} = n_{vis}^2 - 1,\ C_{IR} = \varepsilon(0) - C_{UV} - 1 \tag{2-7}$$

where n(ω) is the index of refraction and ε(0) is the static dielectric constant.

For such materials that spectral optical properties are not available, the Hamaker constant can be also estimated by the Tabor-Winterton approximation (TWA) [17] or single oscillator approximation [18]. The TWA is based on the assumption that the primary contribution to the vdW force results from interband transitions in the visible and

UV range. A typical characteristic absorption frequency of $3x10^{15}$ Hz is used in the TWA. Since the strongest contribution were found to be the high-frequency dielectric responses, the Hamaker constant between Materials 1 in the Medium 3 can be simplified [16] as Equation 2-8.

$$A_{131} = \frac{3kT}{4}\left(\frac{\varepsilon_1(0)-\varepsilon_3(0)}{\varepsilon_1(0)+\varepsilon_3(0)}\right)^2 + \frac{3\hbar\omega_e}{16\sqrt{2}}\frac{\left(n_1^2-n_3^2\right)^2}{\left(n_1^2+n_3^2\right)^{3/2}} \tag{2-8}$$

where ε is the dielectric constant, ω is the plasma frequency, and n is the index of refraction in the visible range. French and co-authors [19] compared the Hamaker constants between identical materials in a vacuum, which were calculated by the TWA and full spectral method. They reported a good agreement between two values for materials with an index of refraction in the range of 1.4-1.8. However, a discrepancy increases for materials with higher indexes because the higher index materials tend to have lower band gap energies, which is neglected with the TWA.

Instead of assuming that the characteristic absorption frequency is constant, the more comparable Hamaker constants for higher index materials can be estimated by varying the absorption frequency with the index of refraction. The Hamaker constant calculated by single oscillator method is expressed as Equation 2-9.

$$A_{121} = \frac{312\left(n_1^2-n_2^2\right)^2}{\left[\left(n_1^2-1\right)^{\frac{1}{2}}+\left(n_2^2-n_1^2\right)^{\frac{1}{2}}\right]\left(n_1^2+n_2^2\right)^{\frac{3}{2}}} \tag{2-9}$$

However, for the nanosize particles, it is very difficult to obtain accurate dielectric spectral parameters over the entire frequency range because quantum effects would influence the dielectric data of the given materials. In addition, the local dielectric

constant of the solvent may be changed because the mobility of the solvent molecules around small ions or particles is restricted in the solvation zone [11].

Retardation and Screening

The electronic magnetic field from the electronic motion within a molecule propagates at the speed of light. When molecules are close together polarization is nearly instantaneous relative to the relaxation time. However, at larger separation distances (>5 nm), the synchronicity between instantaneous dipoles becomes less efficient, i.e., the phase lag between the alignment of dipoles takes place, and thus vdW attraction between two atoms is less, decreasing as D^{-8}, which is known as *retardation*. Additionally, the relative contribution of the permanent dipoles to the total van der Waals attraction increases as separation distance increases. Casimir and Polder [20, 21] first brought up the idea of retardation and they pointed out that contribution of the dispersive part of the Hamaker constant decreases as the separation distance gets larger and the nondispersive part becomes important. Even though the numerical solution to the full Lifshitz equation accounting for the retardation was calculated by Pashley [22], this solution also requires the full dielectric spectra and several simple approximations were given such as correction factor for retardation $f_{retard}(D)$ [23]

$$f_{retard}(D) = \left(1 + \left(\frac{n_3\sqrt{n_1^2 + n_3^2}}{4\sqrt{2}}\frac{D\pi\omega_{UV}}{C}\right)^{\frac{3}{2}}\right)^{-\frac{2}{3}} \tag{2-10}$$

where n_1 and n_3 are indices of refraction in the visible region for the interacting bodies and medium, ω_{UV} is the UV characteristic absorption frequency, and C is the speed of light.

The presence of free charges in a medium also can affect the total vdW interaction in that they reduce the electric field between two bodies. The screening effect by salt ions primarily affects the non-dispersive component of the total interaction over short separation distances because the typical plasma frequencies of ions at 0.1 M salt concentration are in the order of 10^{12} rad/s and the dispersive terms are evaluated at frequencies higher than 10^{14} rad/s. A screened electric field decays exponentially with the separation distance and the screened non-retarded Hamaker constant, A_{screen} was given by Mahanty and Ninham [16]

$$A_{screen} = A_{\omega=0}\left(2\kappa H\right)e^{-2\kappa H} + A_{\omega>0} \tag{2-11}$$

where $A_{\omega=0}$ is zero frequency Hamaker constant, and $A_{\omega>0}$ is Hamaker constant calculated by dispersion contribution, κ is a characteristic inverse length, called Debye-Hückel parameter (κ^{-1} is called Debye screening length). Note that the screening effect is weak since it only affects the static part of the Hamaker constant; and relatively high salt concentrations are required for a substantial change.

Geometry: The Derjaguin Approximation

The interaction between two bodies can be separated by factors depending on the geometry of the interacting bodies as well as material parameters. In 1934, Derjaguin [24] proposed a simple approximate expression for the interaction force between two interacting bodies relating to the interaction energy per unit area between two plates when the radius of sphere is much greater than the interacting distance (R>>D).

$$F(D)_{sphere/plate} = 2\pi R \cdot W(D)_{plate/plate} \tag{2-12}$$

This approximation is useful for the surface force measurement because it is easier to measure the forces experimentally rather than interaction energy and it allows

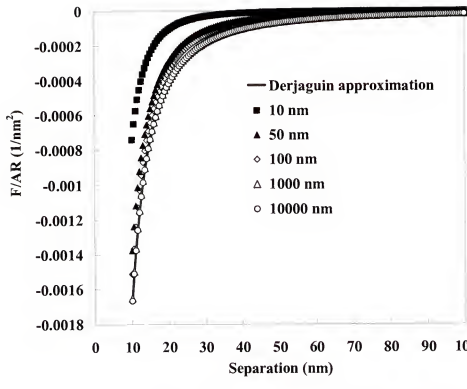

Figure 2-1. Normalized vdW forces between a sphere and a plate as a function of separation distance for spheres with different radii using Equation 2-13. Solid line is calculated by assuming that the size of sphere is much greater than the separation distance (Derjaguin approximation).

comparison between bodies of different geometries. Typically the surface force is normalized by the radius of interacting sphere and the force divided by radius is equivalent to the energy per unit area.

The validity of the Derjaguin approximation can be estimated by the exact analytical expression derived by Hunter [25] and Russel [23].

$$F(D)_{sphere/plate} = -\frac{A}{3}\frac{2R^3}{D^2(2R+D)^2} \xrightarrow{R>>D} F(D)_{sphere/plate} = -\frac{AR}{6D^2} \qquad (2\text{-}13)$$

Figure 2-1 shows the normalized vdW force between sphere and plate for different sphere radii. It is clearly seen that the Derjaguin approximation deviates significantly for small

spheres. This is an important indication in that the Derjaguin approximation can be applied only for sphere whose radius is larger than 500 nm.

Electric Double Layer Force

Situations where only vdW force acts are restricted to a few simple systems, for example, interactions in a vacuum. vdW forces between similar materials are normally attractive with the exception of negative Hamaker constant, inducing a coagulation. However, when particles are immersed in a polar liquid such as water, the electrical charges are developed at solid/water interface. If the charges are of same sign, there is repulsion between particles and coagulation can be prevented. This force is called *electric double layer (EDL) force* and origin of these charges and a few of theories are discussed in the following sections.

Charging of Surfaces

The main sources of electrical charges on the surface are the direct ionization of surface groups, specific ion adsorption, differential ion solubility, and substitution of surface atoms [25]. The driving force for developing charges on the solid surface is thermodynamically due to Gibbs free energy. Unstable atoms at interfaces try to lower their Gibbs free energy through combination with the surrounding molecules. For example, oxides and carbides often form surface hydroxyl and carboxylate groups by hydration in aqueous solution. Such surface hydroxyls react as amphoteric sites and may dissociate or adsorb ions in the solution. This dissociation or adsorption follows the reaction rate equation in the below

$$MOH_2^+ \xleftarrow{K_1} MOH + H^+ \tag{2-14}$$

$$MOH \xleftarrow{K_2} MO^- + H^+ \tag{2-15}$$

where M represents a metal ion at the surface and H^+ and OH^- are potential determining ions because the magnitude of the surface charge is affected by these dissolved ions. Even though real particles have more complicated atomic compositions or different local molecular structure, which result in variation of actual constant, there is a general trend for dissociating materials in water, for instances, surface charge is negative at high pH and positive at low pH.

One of the most important mechanisms which give rise to the development of surface charges is adsorption of dissolution of specific ions due to their different affinity at liquid/solid interface. Charging of many salts such as AgI, CaF_2, and NaCl takes place through this mechanism. For example, AgI has a net negative charge due to the higher dissolution of silver ions at surfaces. Typical example of substitution of surface atoms is the liberation of alkali ions from the surface of clay such as kaolinite. In this case, aluminum ions can substitute for silicon ions, which lead to a negative surface charge.

Once the surface of solid is electrically charged by the above mechanisms, which are normally occur simultaneously, this will be interacting with the other ions in the surrounding solution.

Point of Zero Charge (PZC)

The point of zero charge (PZC) is defined as the pH at which the net surface charge of the bare solid body equals to zero. This term is often used same as the isoelectric point (IEP), but strictly speaking, IEP is the pH where the particles with the adsorbed species is not affected by an external electric field. Thus, PZC and IEP are coincident in the absence of specifically adsorbing species such as multivalent ions. For a simple oxide, which has only one type of surface hydroxyl group, PZC can be calculated in terms of relations (2-14) and (2-15).

$$PZC = \frac{pK_1 + pK_2}{2} \tag{2-16}$$

Parks [26] tried to formulate the relation which can estimate the IEP of the various materials by considering the valence and radius of ions. He found the relation for different type of oxides,

$$pH_{IEP} = 18.6 - 11.5 \cdot (Z/R)_{eff} \tag{2-17}$$

where Z is the valence of cation and R is the sum of cation and oxygen ion radius. In general, the lower the valence of the cation is, the higher the IEP is.

Electric Double Layer (EDL)

Those charges developed at the surface with an electrostatic potential Ψ_0 can be neutralized by the ions of opposite charge, so called counter-ions, dissolved in the surrounding media. This model was first proposed by Helmholtz and the first layer at the interface (inner Helmholtz plane) starts to attract the counter-ions forming the second layer (outer Helmholtz plane). According to this model, there will be a linear drop of the electrical potential from ψ_0 at the surface to zero at the center of the counter-ion layer. However, there are many experimental observations which cannot be explained by this model such as electrophoresis.

Rather, Gouy [27] and Chapman [28] treated this problem as that counter-ions will redistribute due to the thermal energy and the concentration will depend on the distance from the surface, that is, there will be a concentration gradient near the surface. Whereas there will be a local excess of counter-ions around the surface, co-ions will have a lower concentration close to the surface than in the bulk solution due to EDL repulsion. Assuming the ions to be point charges without interactions between them, the charge distribution can be described following the Boltzmann's distribution,

$$\rho_x = \rho_0 \exp(-\frac{Ze\psi_x}{kT}) \tag{2-18}$$

where ρ_x is the number density of ions of valence Z at any point x between two surfaces (ρ_0 is for midpoint, i.e. bulk concentration), and ψ_x is the electrostatic potential at position x. This charge distribution is referred to as the *diffuse layer*.

Combining Equation 2-18 and the Poisson equation for the net charge excess (2-19), the electrical potential at any point in the diffuse layer can be obtained from the Poisson-Boltzmann (PB) equation (2-20)

$$Ze\rho_x = -\varepsilon_r\varepsilon_0(\frac{d^2\psi_x}{dx^2}) \tag{2-19}$$

$$\frac{d^2\psi_x}{dx^2} = \frac{2nZe}{\varepsilon_r\varepsilon_0}\sinh(\frac{Ze\psi_x}{2kT}) \tag{2-20}$$

where e is the electron charge, Z is the valence, n is electrolyte concentration, and ε_0 and ε_r is the dielectric permittivity of vacuum and the dielectric constant of the solvent, respectively.

The PB equation is a non-linear second-order equation and two boundary conditions are required to solve the equation between two charged surfaces. The first boundary condition is that the electrical field must be zero at the midpoint and the second boundary condition is the electroneutrality of the system. For a z:z electrolyte solution, Equation 2-20 can be simplified with mathematics;

$$\frac{d\psi}{dx} = -\frac{2\kappa kT}{Ze}\sinh\left(\frac{Ze\psi}{2kT}\right) \tag{2-21}$$

This relation can be again integrated to yield

$$\psi_x = \frac{4kT}{Ze} \ln \left[\frac{1 + \exp(-\kappa x) \tanh(\frac{Ze\psi_0}{4kT})}{1 - \exp(-\kappa x) \tanh(\frac{Ze\psi_0}{4kT})} \right] \tag{2-22}$$

where ψ_0 is the Stern potential and κ is the reciprocal Debye screening length. At low potentials, tanh(x) can be substituted h(x), reducing to the Debye-Hückel equation

$$\psi_x = \psi_0 \exp(-\kappa x) \tag{2-23}$$

Although the Gouy and Chapman model is valid to describe a part of the interface, it is still necessary to consider the presence of ion binding to the surface. Stern [29] and Grahame [30] developed an extended model combining two models described above. This is known as the electric double layer (EDL) model which is composed of Stern and the diffuse layer as illustrated in Figure 2-2. In Stern layer, counter-ions are strongly adsorbed and lower the electric potential at points adjacent to the particle surface. The difference from the Helmholtz theory is that the number of counter-ions adsorbed to the surface is assumed to be proportional to the surface potential and bulk electrolyte concentration. If the dielectric constant is uniform (ε_δ), the Stern layer can be treated as a capacitor and the potential drop across the layer from a surface potential ψ_0 to a Stern or outer Helmholtz potential ψ_δ is given by

$$\psi_\delta = \frac{\sigma_0 \delta}{\varepsilon_\delta \varepsilon_0} \tag{2-24}$$

where δ is the thickness and ε_δ is the relative dielectric constant of the Stern layer. The charge per unit area at the Stern layer σ_δ can be described with the surface potential, which is called Grahame equation

$$\sigma_\delta = \sqrt{8\varepsilon_r \varepsilon_0 Z^2 nkT} \sinh(\frac{Ze\psi_0}{2kT}) \tag{2-25}$$

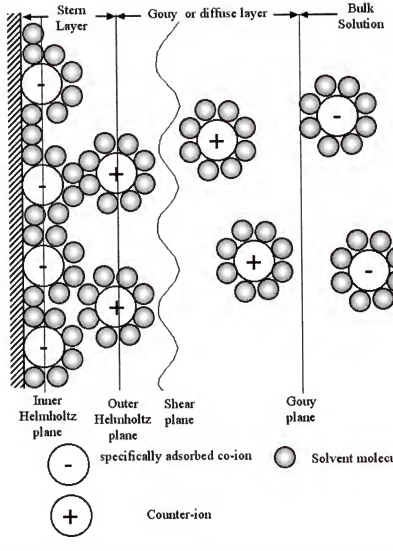

Figure 2-2. The electric double layer (EDL) model developed on the charged surface. The surface due to the presence of charge has a potential Ψ_0. The outer Helmholtz plane (OHP) is the closest distance that counter ions can come to the surface. The value of the potential at shear plane is called zeta potential (Ψ_ζ).

Equation 2-25 can be simplified for low potentials to

$$\sigma = \varepsilon_r \varepsilon_0 \kappa \psi_0 \tag{2-26}$$

and can be interpreted as a capacitor with a thickness of $1/\kappa$ from the Equation 2-24. This thickness or characteristic length is known as Debye screening length, which is the inverse of the Debye-Hückel parameter κ, is expresses as

$$\Lambda = \kappa^{-1} = \left(\frac{2nZ^2e^2}{\varepsilon_r \varepsilon_0 kT} \right)^{-\frac{1}{2}} \tag{2-27}$$

Debye length κ^{-1} in aqueous solution at 25°C is a function of the concentration and valence of the electrolytes. For example, for NaCl, κ^{-1}=30.4 nm at 10^{-4} M, 9.6 nm at 10^{-3} M, 0.96 nm at 0.1 M, and 0.3 nm at 1 M.

The solution of Equation 2-20 can be obtained differently depending on the particle size and surface potential as shown in the Table 2-2 [31]. If the particle size is large, the double layer can be treated as flat and Cartesian coordinates are applied. However, the double layer must be considered as spherical for nanoparticles.

Although surface potential or Stern potential can be obtained by a potentiometric technique, this method is rather tedious and has several systematic errors. A simple alternative method is to measure the potential on the particle directly. The zeta potential measurement is one of these techniques.

Table 2-2. Solution to the PB equation for high and low surface potentials in a symmetric electrolyte for high and low surface curvature.

	κa >>1	κa <<1
$\psi_s < 25$ mV	$\psi(x) = \psi_1 \exp(-\kappa x)$	$\psi(r) = \frac{a\psi_1}{r}\exp(-\kappa(r-a))$
$\psi_s > 25$ mV	$\tanh(\frac{y}{4}) = \tanh(\frac{y_0}{4})\exp(-\kappa x)$ where $y = \frac{ze\psi}{kT}$ and $\kappa = \left(\frac{2z^2e^2n^\infty}{\varepsilon_r \varepsilon_0 kT} \right)$	$\nabla^2\psi = \frac{d^2\psi}{dr^2} + \frac{2}{r}\frac{d\psi}{dr}$ $= \frac{2zne}{\varepsilon_r \varepsilon_0}\sinh(\frac{e\psi}{kT})$

Zeta Potential

Phenomena related to the motion of one phase relative to the other phase with charges are termed as *electrokinetic effects* including electrophoresis, electroosmosis,

streaming potential, and sedimentation potential [25]. When charged particles in a suspension respond to the external electric field, they are forced to move relative to the surrounding media, which is called *electrophoresis*. Electrophoresis is the most important phenomenon since it can be measured directly for the charged particles.

As shown in Figure 2-2, there is a boundary beyond which counter-ions do not move with the particle. This boundary is defined as a slip plane or plane of shear. The slip plane is often assumed to be located in the range of 0.4 nm to 2 nm from the surface, which is quite small compared with the Debye length. Since the double layer structure is disturbed at the slip plane, there is a potential difference between the slip plane and the bulk solution, which is known as *zeta potential*. Undoubtedly, zeta potential is different from the surface potential ψ_0 due to the inner layer of adsorbed counter-ions, but is often considered same as the Stern potential ψ_δ for a low ionic strength solution and low potential surface.

Zeta potential can be estimated by the balance between the electric force and viscous force (Stokesian flow) of the particles in the liquid. For a large particle having a thin double layer ($\kappa R>100$, i.e., high ionic strength), Smoluchowski [32] derived the relation between the particle mobility and zeta potential

$$\zeta = \frac{\eta}{\varepsilon_r \varepsilon_0} \mu_E \tag{2-28}$$

where ε_r is the relative dielectric constant of the medium, ε_0 is the permittivity of free space, η is the viscosity of the medium, and μ_E is the electrophoretic mobility of the particle. For particles with a thick double layer such as nanoparticles ($\kappa R<1$), a similar equation as Smoluchowski was derived by Hückel [33]

$$\zeta = \frac{3\eta}{2\varepsilon_r \varepsilon_0} \mu_E \tag{2-29}$$

The relation of zeta potential and mobility of particle between these two limits was proposed by Henry [34] dividing Equation 2-29 with a correction factor f(κR).

EDL Interaction between Charged Surfaces

In the above, isolated and charged surfaces are considered. When the surfaces of same charge interact with each other, the repulsive interaction can be analyzed by considering the free energy change and the osmotic pressure generated by the accumulation of ions between the particles. The increased ionic concentration decreases the entropy and changes the charge on the surface.

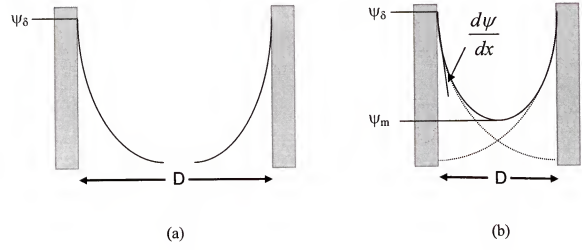

Figure 2-3. Potential profile versus separation between two opposing electric double layers. Solid line represents the anticipated potential distribution with minimum at midplane.

A schematic drawing of two interacting double layers is shown in Figure 2-3. For most cases, only the diffuse layers interact with each other and the potential on the surface is assumed to be the Stern potential, ψ_δ. Whereas the EDL does not overlap at

large separation (Figure 2-3 (a)), the potential profiles are changed at shorter separation (Figure 2-3 (b)).

Boundary Conditions for Calculating EDL Forces

There are two limiting situations for double layer interactions. From Equation 2-24, it can be presumed that if ψ_δ is constant during the compression of the two layers then the derivative of the potential at the surface $d\psi/dx$ will decrease corresponding to decreasing charge. This implies that both counter- and potential determining ions locally increase at the surface when double layers overlap. These accumulating counter- and potential determining ions will decrease exponentially surface charges at smaller separation. This is called a *constant potential boundary condition* and especially surfaces charged by adsorption of ions tend to have constant potential. Due to the charge decrease at any given separation, this boundary is expected to yield the lower limit for magnitude of EDL force.

If, on the other hand, the charge is constant during compression, which means that $d\psi/dx$ is constant, the potential must decrease to zero at small separation. This is called a *constant charge boundary condition* and surfaces with permanently charged groups such as lattice defects, which are not much affected by the concentration of counter-ions, are expected to approach this limit. This boundary condition predicts the upper limit of EDL force.

Practically, however, both conditions are not likely to occur in real surfaces. For example, the interaction of surfaces charged by an acid-base reaction will affect the degree of dissociation of surface groups, which is dependent on the local concentration of counter-ions. This is called *charge regulation* [25]. Thus, the repulsion between these

charge-regulated surfaces lies between the two limits of the above. The charge regulation condition is more significant at short separation distance, and for a larger separation, three interaction curves can converge into a single analytical expression. Although the Poisson-Boltzmann equation may break at small separation distance, these boundary conditions are still useful to calculate EDL forces and estimate the interaction between charged surfaces.

The analytical calculation of the Poisson-Boltzmann equation was performed by Hogg et al. [35], which is known as Hogg-Healy-Fuerstenau (HHF) equation. For two opposing plates under a constant potential boundary condition, the interaction energy between them is expressed as

$$W_{\psi}(D)_{plate/plate} = 2Z^2 nkT\left(\frac{e\psi_{\delta}}{kT}\right)^2 \frac{1}{\kappa}\left(1-\tanh\frac{\kappa D}{2}\right) \tag{2-30}$$

where Z is the valence of counter-ions, n is the number density of counter-ions, kT is the product of Boltzmann's constant and absolute temperature, e is the electron charge, ψ_{δ} is the Stern potential, κ is the reciprocal Debye length, and D is the distance between two surfaces. The interaction energy under a constant charge boundary condition also can be written as

$$W_{\sigma}(D)_{plate/plate} = 2Z^2 nkT\left(\frac{e\psi_{\delta}}{kT}\right)^2 \frac{1}{\kappa}\left(\coth\frac{\kappa D}{2}-1\right) \tag{2-31}$$

Equations (2-30) and (2-31) can be expressed as another equation for low potential and low ionic strength conditions.

$$W_{\psi}(D)_{plate/plate} = W_{\sigma}(D)_{plate/plate} = \frac{64nkT}{\kappa}\tanh^2\left(\frac{Ze\psi_{\delta}}{4kT}\right)\cdot\exp(-\kappa D) \tag{2-32}$$

This interaction is valid at low degrees of double layer overlap (D>1/κ), which is known as the *weak overlap approximation* [11]. Simple expression for the EDL repulsive energy between two approaching spheres of radius a is also given by

$$W_{rep}(r) = \frac{4\pi\varepsilon_r\varepsilon_0\psi_\delta^{\,2}a^2}{r}\exp\left[-\kappa a\left(\frac{r}{a}-2\right)\right] \tag{2-33}$$

For higher potentials and shorter separation distances, the extended power series approximation of Poisson-Boltzmann equation has also been used [36]. However, this analytical solution is still not satisfying the description of the EDL force at high potentials (> 60 mV). Thus, a full non-linear numerical solution is required at high surface potential and short separation distance.

DLVO Theory

vdW and EDL forces are the main forces that particles suspended in a solution can experience. So the summation of those to interaction should give a very good prediction about the interparticle forces. That concept was developed by Derjaguin-Landau-Verwey-Overbeek and is known as DLVO theory [37, 38]. The total energy in a particle system can be expressed by the summation of vdW and EDL energies

$$W_{total} = W_{vdW} + W_{EDL} \tag{2-34}$$

This simple equation has predicted well the behavior of particulates in solution for a variety of conditions and been proven to be valid with the majority of colloidal materials. The normal criterion is that a barrier of 25 kT is sufficient to achieve colloidal stability.

Even though DLVO theory is universal and mostly accepted to describe the macroscopic colloidal behavior, there are a number of examples where it does not adequately interpret the measured interaction profiles. Since DLVO is based on a

continuum approach, neglecting solvent effects such as ion-solvent interactions, surface-solvent interactions, and ion-ion correlation, non-DLVO forces occur when the property (e.g. density and mobility) and molecular structure of solvent near surfaces of particles are different from the bulk property [39]. The existence of these forces to explain the stability of the fine powders has been confirmed with the development of surface force measurement techniques. For example, it was first observed by Horn [40] that oscillatory solvation (or hydration in water) forces occur between smooth surfaces such as mica at very short separation distances due to the overlap of two solvated surfaces, which arise from the specific solute-solvent and modified solvent-solvent interactions. Alternatively, attractive hydrophobic forces may occur due to the unfavorable structure of water (i.e. rearrangement of H-bond) near an interface [11].

Total interaction energy between two approaching spheres is plotted as a function of particle size in Figure 2-4. It shows clearly dependence of the interaction energy on the particle size. The interaction energy increases with particle radius and barrier height of the colloidal stability consequently increases as the particle size increases. In other words, as particle size decreases, a greater Stern potential is needed to prevent coagulation. However, the primary and secondary minimum associated with particle coalescence also becomes deeper as the particle size increases. Thus, the range and magnitude of the total interparticle forces is essential in controlling the stability of the given particles. If relatively large particles coalesce in solution, they will not be separated again since their thermal energy will be insufficient to move out of the primary minimum. Nanosized particles are theoretically easy to decoagulate due to small primary minimum even though the repulsive barrier is small for nanoparticles. However, kinetics

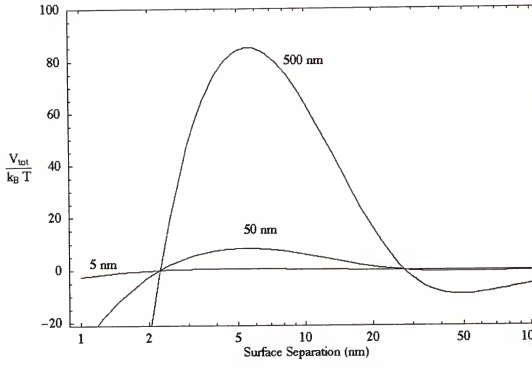

Figure 2-4. The calculated total interaction energy (Equation 2-34) between two spheres as a function of the surface separation from micrometer to nanometer size regime of diameter. The repulsive energy was calculated from Equation 2-33 and parameters used are $\psi_\delta = 25$ mV, $\kappa^{-1} = 100$ Å. The nonretarded vdW attractive energy was calculated from Equation 2-3 and the Hamaker constant A is 6×10^{-20} J.

of decoagulation is more important in practical applications of nanoparticles [31]. If it is slow, the temporary agglomerate of nanoparticles behaves like a large particle and the vdW interaction energy will gradually increase and they will be hard to be dispersed. From this theoretical calculation, it is clear that stabilization by small molecules such as adsorbed polymer or surfactant is much more efficacious for nanoparticles than for larger colloidal particles. However, the effect of the repulsive layer thickness on the packing density of nanoparticles has to be considered. A thick repulsive layer is better for stabilization of particles but it will reduce the achievable packing density [41]. Thus, in

order to achieve stable high solids loading slurries, optimal thickness has to be just sufficient to prevent aggregation and minimize the occupied volume.

Steric Force

Polymeric dispersant molecules or polyelectrolytes have been widely used to control the stability in many industries such as ceramic processing, paper, and cosmetics [42]. Polymeric molecules are more effective in stabilization because the greater level of electrolytes can be tolerated, the electroviscous effect is reduced, and higher solids loading is possible [43]. When the polymers are added they start to adsorb on the surface in order to minimize the total energy. When particles come close and the chains try to penetrate each other the entropy is reduced dramatically. Consequently this effect, known as *steric force*, prevents particles from coming in distance less than the gyration radius of the polymer. Steric force is more important in non-aqueous systems because EDL stabilization is usually not very effective in such situations. For polyelectrolytes, another term *electrosteric force*, which is the combination of EDL and steric force arising from the charged polymers, is often used. Interaction force between the particles adsorbed with polyelectrolytes can be described by the EDL force at larger separation distance because polymer chains on one surface do not interact with chains on the other surface. At shorter interaction range, forces originating from polymers are more important. In further detail, the conformation of the polymer is also important in determining the interactions between them. The adsorption and conformation of polymers on the surface of the particles depends on a number of parameters in the system such as the solvency of the solution, relative charge of polymer and particles as well as pH and ionic strength [23].

Polymers in Solution

The interaction range between polymer-coated surfaces can be estimated from the dimension of polymer molecules. The behavior of polymers in solution is different before they are adsorbed or grafted to the surfaces. The most acceptable theory describing the movement of polymer chain in solution is the random walk model first introduced by Kuhn [44]. In this model, the polymer chain is composed of the repeated N segments of a monomer having an effective length l. An end-to-end vector R is here introduced to describe the characteristic size of the polymer. If the segment-segment interaction of the polymer in a solvent is zero, which is called an ideal solvent, polymer behavior can be described by a stepwise diffusion process under Brownian motion. Conveniently, the mean square end-to-end distance is introduced by averaging products of one individual segment vector with one another.

$$\left\langle R_0^2 \right\rangle = \sum_{j=1}^{N} \sum_{i=1}^{N} \left\langle \vec{l}_i \bullet \vec{l}_j \right\rangle = N \cdot l^2 \tag{2-35}$$

The radius of gyration R_g, which is the root mean square distance of the segments from the center of mass, is defined by [45]

$$R_g = \sqrt{\frac{\left\langle R_0^2 \right\rangle}{6}} = \frac{l\sqrt{N}}{\sqrt{6}} \tag{2-36}$$

However, real chains are not completely flexible and their movement is hindered due to fixed bond angles and confined rotation about the backbone chain. Thus, Flory [46] introduced a characteristic ratio C_∞, which is the ratio of the actual dimensions to ideal dimensions of the chain and Equation 2-38 can be modified to

$$\left\langle R_0^2 \right\rangle = C_\infty N \cdot l^2 \tag{2-37}$$

Another way to describe the chain stiffness is the wormlike model. In this model, the *persistence length* L_p is defined as a characteristic length along the chain over which directional correlation between the segments disappears [45]. The value of the persistence length is almost infinite for a rigid polymer whereas it is slightly larger than l for a very flexible polymer. For the intermediate region, R_0 can be expressed by

$$\left\langle R_0^2 \right\rangle = 2L_p L - 2L_p^2 \left[1 - \exp\left(-\frac{L}{L_p} \right) \right] \tag{2-38}$$

where L is the contour length of polymer that is equivalent to $N \cdot l$.

Excluded Volume

The above equation is based on ideal solvent ignoring the interaction between the segments and effect of solvent. The relation between the solvent and segment can be depicted by the *Flory-Huggins parameter* χ which is defined as the energy change to transfer segment from pure polymer to pure solvent (or vice-versa). If solvent and polymer segments have same polarity and polarizability, χ is zero, in which solvent is called good or athermal. In that case, polymers will have a large chain expansion due to volume exclusion.

The excluded volume can be written as νl^3 where ν is dimensionless excluded volume parameter and is defined as

$$\nu = 1 - 2\chi \tag{2-39}$$

If χ=0.5, then ν is zero, chains behave ideally and this condition is called θ-point. Polymer chains behave ideally in θ-solvent (or ideal solvent) and polymer size is considered to be R_g ($\propto N^{0.5}$).

For non ideal solvent, polymer size can be defined by the *Flory radius* R_F, which is given as

$$R_F = \alpha R_g = l \cdot N^{\nu} \tag{2-40}$$

where α is a linear expansion coefficient. For ideal solvent, α=1 and ν=0.5. Polymers expand in good solvent corresponding to α>1 and ν=0.6. Finally, polymer chains coils in poor solvent due to attraction between monomer segments. However, it should be noted that solution properties can be transformed into each other by adding another solvent or salt as well as changing solvent temperature.

Polyelectrolytes in Solution

As a polyelectrolyte is dissociated, the repulsion between the charged chains will induce the polymer to become rigid. Total persistence length L_{pt} is the sum of intrinsic L_{p0} and electrostatic persistence length L_{pe}. The effect of charge can be evaluated by comparing the average distance between charges along the chain l_e with Bjerrum length l_B is given by [45]

$$l_B = \frac{e^2}{4\pi\varepsilon_r\varepsilon_0 kT} \tag{2-41}$$

which is the distance between two monovalent ions at which their Coulombic energy is equal to kT. Depending on degree of ionization, effective distance between the charges l_{eff} is assumed to be l_e at low charge density and zl_B at high charge density, z being the valence of monomer charge.

$$L_{pe} = \frac{l_B}{4}\frac{1}{\left(l_{eff}\kappa\right)^2} \tag{2-42}$$

Electrostatic persistence length decreases with increasing salt concentration, which means that polyelectrolyte becomes flexible at low salt concentration. On the other hand, $1/\kappa$

goes to zero at high salt concentration and polyelectrolytes behave like their uncharged counterparts.

Polymer Layers on a Surface

The configuration behavior of the polymer near a solid surface is more complicated not only because the interaction between each other and solvent but also interaction with the surface must be considered. Polymer chains can be adsorbed via physical forces (physisorption) or by grafting via specific chemical bonds (chemisorption). Different configuration structures are possible depending on the nature of polymer and bulk polymer concentration as well as bonding between polymer chain and solid surface. For example, for grafted polymers with low concentration, in which distance between two grafting points s is larger than the chain dimension, the possible structure is *mushroom* or *pancake* structure corresponding to weak or strong adsorbing segments, respectively. If, on the other hand, grafting density is high and s is smaller than the chain length, chains will be stretching out, which is called *brush* structure. The various types of polymer structure on the surface are shown in Figure 2-5.

The concentration profile of monomer segments for a mushroom configuration has a Gaussian shape and the equilibrium height of the mushroom layer is in the order of the chain dimension in solution [47]. Using a self consistent mean field theory, Milner [48, 49] showed that the concentration profile of brush configuration in good solvent forms a parabolic shape and height L_b is expressed as

$$L_b = Nl\left(\frac{12}{\pi^2}\right)^{\frac{1}{3}}\left(\nu\sigma l^2\right)^{\frac{1}{3}} \tag{2-43}$$

where N is the number of monomer segments, l is effective length, ν is the excluded

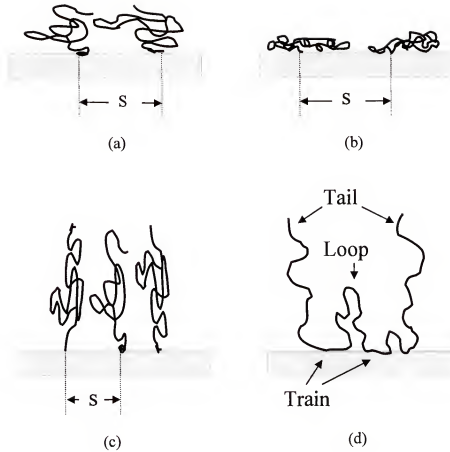

Figure 2-5. Typical polymer structures on the surface. (a) mushroom (b) pancake (c) brush configurations. S denotes the distance between the grafted points. (d) adsorbed polymer.

volume parameter, and σ is the number of grafted chains per unit area, which is related to the mean distance between the grafted points, s, by $\sigma=1/s^2$. As seen in the Equation 2-43, the brush height scales with the molecular weight and grafting density.

Unlikely to the grafted polymer, in which the most segment parts are not adsorbed except for an anchoring segment, the physically adsorbed polymer has more adsorbing points between the polymer chain and the surface. The configuration of adsorbed polymers is typically termed *loop, tail*, and *train* depending on the attraction between the

segments and surface as shown in Figure 2-5 (d). The overall density profiles of the adsorbed polymer will be determined by the relative proportions and lengths of these structural elements. According to the self consistent field lattice theory [45], density of the monomer segments decays following the power law of the distance from the surface.

Interaction between Polymer Coated Surfaces

The interaction features of particles are dependent on a variety of parameters such as the nature of bonding between the segment and the surface (i.e. grafted or adsorbed), and the coverage of the added polymer on the surface, and quality of the solvent. The interaction force theories between the surfaces carrying grafted polymers have been developed relatively well. The interaction force between a sphere and a plate having a mushroom configuration is given by [47]

$$\frac{F(D)}{R} = 2\pi \frac{3kT\sigma}{5}\left[\left(\frac{2L}{D}\right)^{\frac{5}{3}} - 1\right] \tag{2-44}$$

where L is the thickness of the adsorbent layer. For a brush configuration, the force is given by [50]

$$\frac{F(D)}{R} = 2\pi \frac{8kTL\sigma^{\frac{3}{2}}}{35}\left[7\left(\frac{2L}{D}\right)^{\frac{5}{4}} + 5\left(\frac{D}{2L}\right)^{\frac{7}{4}} - 12\right] \tag{2-45}$$

The interpretation of the interaction force between the adsorbed polymer layers is more complicated because adsorbed layers are highly dynamic, with the individual segments continually attaching and detaching from the surface corresponding to the change in the concentration of profile of loop and/or tail configuration.

Macroscopical behavior of colloidal system is affected by the concentration of the polymer. When the concentration is low and not sufficient to cover the surfaces of

particles, polymer bridging may occur, where one polymer chain adsorbed on the one surface attaches to another particle. The result will be the flocculation of the particles. If the polymer concentration keeps increasing beyond full surface coverage then another effect takes place. When the excess polymer exist in the solution and the fully coated particles approach closer (i.e. < radius of gyration), non-adsorbed free polymers between them start to be excluded due to entropic effects. Eventually the local concentration becomes lower than the surrounding. The concentration difference creates osmotic pressure difference that attracts two particles. This is known as the depletion flocculation. If the concentration increases even more then, the polymer actually becomes the solvent and the depletion effect is reversed. The particles are pushed apart and the system is stabilized. This effect is known as depletion stabilization.

Surface Force Measurement Techniques

Stability of the particular colloidal system can be investigated in several ways such as turbidity [51, 52], sedimentation [53, 54], electrokinetics [55], viscosity [56, 57], etc. Among them, surface force measurement technique has been a useful method to directly characterize the interaction between particles. Several techniques for measuring interaction forces between macro- and microscopic surfaces have been developed including surface force apparatus (SFA) [17, 58], total internal reflection microscopy (TIRM) [59], and atomic force microscopy (AFM). Each technique has unique advantages over the others. For example, SFA has an ability to determine the true separation distance and TIRM is able to detect very small forces down to 10^{-14} N. However, these two methods can be utilized only for special surfaces. On the other hand, AFM has the merit in that almost all materials can be investigated including hydrophilic and hydrophobic surfaces, and biological molecules.

Atomic force microscopy (AFM) was developed as an imaging tool of surfaces in atomic scale in the late 1980s [60]. The use of the AFM in surface force measurement has been popular since Ducker introduced the colloidal probe technique, where a well defined single colloidal particle was attached to the cantilever [61]. Since the interaction surface area is smaller than SFA, this technique is less sensitive to the surface contamination and has a relative simple experimental setup procedure. Force sensitivity is about 10^{-12} N and distance resolution is 0.1 nm scale. A schematic drawing of AFM force measurement is shown in Figure 2-6. Operation principle is simple. The piezoelectric scanner on which the sample is located approaches the probe, which is attached to the sensitive cantilever. As they come close, the cantilever spring will bend upward or downward depending on the nature of interactive force between them. Degree of bending is measured by the deflection of laser, which is reflected to a quadrant photodiode detector above the cell.

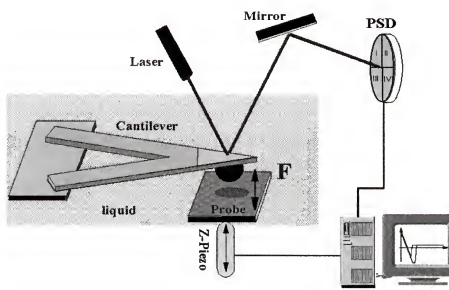

Figure 2-6. Standard colloidal probe technique for measuring directly interaction force between surfaces in the liquid cell mode of the AFM.

Conversion of Raw Data to Force-Separation Curves

A raw data of the applied piezoelectric voltage versus detector signal and the conversed force-separation curve are shown in Figure 2-7. At region (I), no force is observed because the separation between the scanner and probe is too far to have an interaction. As the scanner approaches further in the region (II), surfaces forces between them cause the cantilever to deflect up or down. If the attraction force is so strong that it exceeds the stiffness of the cantilever, the probe jumps into the sample surface. The lower the spring constant, the higher the sensitivity is. However, it should be noted that the region where attractive forces can be measured becomes narrower with a low spring constant cantilever. After a probe jumps in and contacts the surface, the cantilever is deflected as much as the movement of the piezo scanner. This linear contact region (III) is called *constant compliance* region, by which a separation distance in the force-separation plot is determined. In a similar manner as approach, deflection of the cantilever decreases upon retraction of the probe. The separation of the probe occurs at the *jump-off* point, from which a maximum adhesion force can be measured (region (IV)).

For a quantitative evaluation, force is calculated by the deflection of the cantilever multiplied by its spring constant, which is equivalent to Hooke's law

$$F = k \cdot \Delta z = k \cdot \left(V - V_0\right)_{\det ector} \cdot \frac{1}{\alpha} \cdot \left(\frac{\Delta z}{\Delta V}\right)_{piezo} \qquad (2\text{-}46)$$

where k is the spring constant of cantilever and $(V\text{-}V_0)_{detector}$ is the detector signal relative to the zero force region, α is the slope of the constant compliance, and $(\Delta z/\Delta V)_{piezo}$ is the sensitivity of the piezoelectric scanner. Therefore, the determination of spring constant is important to obtain the accurate interaction force. Since AFM cantilevers are made by

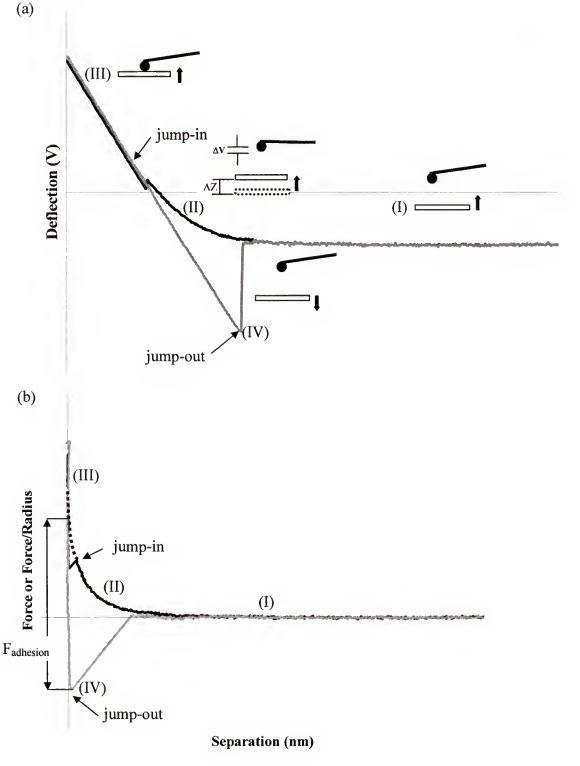

Figure 2-7. Surface forces measured with an AFM colloidal probe technique. (a) A deflection signal of the cantilever versus a piezo scanner displacement with the cartoon of the motion of cantilever when substrate is engaged and disengaged. (b) A converted force versus separation distance plot.

microfabrication techniques such as evaporation and etching, the actual spring constant is different from batch to batch. There are several types of techniques for the determination of spring constant, which will be described in the following.

Determination of Spring Constant

The spring constant of the cantilever can be estimated by the geometrical calculation. Sarid [62] and Sader [63] proposed a simple expression for an end-loaded rectangular and triangular V-shaped cantilever, respectively

$$k = \frac{3EI}{L^3} = \frac{3Ewt^3}{4L^3} \qquad \text{for rectangular} \tag{2-47}$$

$$k = \frac{Et^3 w}{2L^3}\cos\theta\left[1 + \frac{4w^3}{b^3}(3\cos\theta - 2)\right] \qquad \text{for triangular} \tag{2-48}$$

where I is an inertia, E is the elastic modulus of spring material, t is the thickness and the additional parameters are given in Figure 2-8.

Figure 2-8. Dimension of a rectangular and a triangular V-shaped cantilever.

Scanning Electron Microscopy (SEM) is normally employed for measurement of these parameters but an experimental error for this method may result in an uncertainty of about ± 20% [64]. Additionally, a reflective metallic coating or elastic modulus that may be different from batch to batch due to variation in stoichiometry of the spring material

will affect the determination of spring constant. Thus, calibration methods irrespective to the dimension or materials property are more desirable.

Hutter et al. [65, 66] measured a spring constant from the thermal vibration of the cantilever in air. Cantilever oscillates at temperature T with an amplitude x_0, so that

$$\left\langle \frac{1}{2} m\omega_0^2 x_0^2 \right\rangle = \frac{1}{2} k_B T \tag{2-49}$$

where m is the effective mass of cantilever, ω_0 is resonant frequency, and k_B is Boltzmann's constant. Since $\omega_0^2 = k/m$, spring constant can be obtained from Equation 2-49

$$k = \frac{k_B T}{\left\langle x_0^2 \right\rangle} \tag{2-50}$$

This method is quite simple and reliable for soft cantilevers but the damping effect in the air may affect the measurement of resonant frequency.

Another method was proposed by Cleveland [67] measuring the change in the resonant frequency due to the added mass of tungsten particle. If the mass of the particle M is known and resonant frequency ν_0 of the unloaded and ν_1 of the loaded cantilever are measured, spring constant can be expressed as

$$k = (2\pi)^2 \frac{M}{\frac{1}{\nu_1^2} - \frac{1}{\nu_0^2}} \tag{2-51}$$

Their technique was accurate to approximately 10% but requires a careful micro position because off-end loading may give different resonant frequency inducing a large uncertainty.

Aside from the above dynamic calibration, the static loading of the cantilever with a precalibrated cantilever or pendulum have also been used [64]. However, these methods are reported to be time consuming and have a relatively larger uncertainty of the measured spring constant. Holbery et al. [68, 69] presented a nanoindentation method to overcome these drawbacks and the accuracy of their method was believed to be within ± 10% for a stiff cantilever.

In this dissertation, the Cleveland resonance frequency and thermal vibration methods were used to determine the spring constant of the cantilevers employed in the experiments.

Summary

Several concepts and theories on surface forces of colloidal particles have been covered in this chapter. The DLVO theory, which is the sum of vdW and EDL force, is a widely acceptable concept to describe and control the interaction between colloidal bodies and is still useful in many practical cases. Additionally, some theories about interactions between the adsorbed polymers at solid/liquid interface were introduced. However, as the particle size comes down to a few nanometers, the scalability of the conventional force theories is questionable. The general operation principle of the AFM colloidal probe technique and a few methods for determining the spring constant of the cantilever were introduced. Based on these backgrounds, the conformation and the interaction forces of the polyelectrolytes adsorbed on colloidal particles from micrometer to nanometer size range will be discussed.

CHAPTER 3
ADSORPTION OF POLYETHYLENEIMINE (PEI) ON SILICA PARTICLES AND DISPERSION BEHAVIOR

Introduction

The control of colloidal dispersion significantly affects the rheology and results in the properties of final products (homogeneity, and packing of particles and distribution of pores). Suspension properties are governed by several important factors such as particle size, particle shape and distribution, viscosity of the suspending media, and the range and the magnitude of particle-particle interactions [23]. In fact, colloidal suspension is thermodynamically unstable and has a tendency to coagulate due to the large free surface energy [70]. However, stable colloidal dispersion can be achieved kinetically by developing an energy barrier to coagulation. If the energy barrier is sufficiently large in magnitude by either EDL or steric repulsion, particles can overcome aggregation resulting from vdW force.

Use of polyelectrolytes as dispersing additives is expanding in colloidal processing because they are very efficient to control the stabilization of particles in liquid media due to the combination of EDL and steric repulsion [71]. Because polyelectrolyte has both electrical charge and polymer chains, adsorption of polyelectrolyte on charged surfaces is determined not only by charge density of the polymer and surfaces, which are of function of several parameters such as pH and ionic strength but also by their molecular weight and concentration, chain conformation, and chemistry of the functional groups.

Polyethyleneimine (PEI) is a branched cationic polyelectrolyte used as a steric stabilizer or flocculant of anionically charged colloidal particles such as SiO_2, SiC [72], and mica surfaces [73] especially under acidic and neutral pH conditions. Extensive studies have been done on the adsorption behavior of the linear type polyelectrolyte such as polyacrylic acid (PAA) [74-76] as a function of pH and ionic strength. However, these effects of branched or starlike polyelectrolyte are less understood. Adsorption of PEI on Ludox silica particles with mean diameter of 14 nm as a flocculant was studied on the effect of charge density and molecular weight by Lindquist et al. [77]. They found that complete adsorption occurred with a concentration required to initiate flocculation regardless of pH and molecular weight. With this concentration, the linear relationship was also found between the logarithm of concentration of PEI and logarithm of charge density of PEI molecules. Akari et al. [78] imaged a single PEI molecule on latex particles using chemical force microscopy. They suggested the "flattening" of the adsorbed PEI molecules by comparing the lateral size and height of adsorbed PEI with size of PEI in solution. Radeva et al. demonstrated that the electro-optic behavior of the Hematite (Fe_2O_3) was governed by the electrical charge of the adsorbed PEI [79]. Recently, pH and ionic strength effect of the dynamic adsorption of PEI on silica substrate as a function of time was investigated by Meszaros et al. using reflectometry [80]. They reported that adsorption plateau of PEI was reached very fast (< 2 minutes) over the entire pH range and adsorption rate was faster at low pH range.

In this work, the systematic studies of PEI adsorption on silica particles were performed as a function of pH, ionic strength, and molecular weight relating to the

electrokinetic response and dispersion. These results will be correlated to the surface force measurement in the next chapter.

Experimental

Materials

SiO_2 powders were purchased from Alfa Aesar with a mean particle diameter (d_{50}) of 0.8 μm that was determined by using a Honeywell Microtrac UPA150 particle size analyzer utilizing dynamic light scattering. A specific surface area of this powder is 2.03 m2/g, which was determined by Brunauer-Emmett-Teller (BET) method using nitrogen.

Polyethyleneimines (PEI, 99 %, Alfa Aesar, MA), with average molecular weights (Mw) of 600, 1,800, and 10,000 g/mol were used in this experiment. PEI is a highly branched and water soluble polymer, which is composed of 1:2:1 ratio of primary, secondary, and tertiary amino groups as shown in Figure 3-1.

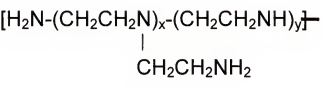

Figure 3-1. Structure of polyethyleneimine (PEI)

Protonation of amine groups of PEI in neutral and acidic pH results in positively charged polymer. According to the potentiometric titration of PEI [81], the ionization degree of PEI is about 10% at pH 10 and 75% at pH 4. Sodium Chloride (NaCl, 99+ %, ACS reagent) was used as a background salt and the pH of the suspension was adjusted with ACS reagent grade hydrochloric acid (HCl) and sodium hydroxide (NaOH).

Methods

The zeta potential of silica particles adsorbed with PEI was measured by zeta reader Mark 21 (ZPI Inc., NJ). Applied voltage to induce particles to respond to electric field was 20 V. 0.3 g of silica powder was mixed with 500 ml solution with 200 mg/L concentration of PEI for each molecular weight. The suspension was ultrasonicated at 50 W for 3 minutes and mechanically stirred for 1 hour. Initial pH of the suspension was about 9.37±0.2 and was increased to about pH 10.7 using 3 N NaOH. Then, pH of suspension was changed with 1 N HCl with the interval of 5 minutes. The suspension was fluxed through the chamber where the particles respond to the electrical field. The movement of the particles inside the chamber can be monitored and zeta potential is determined by matching the electrical field lines with the mobility of particles at the same velocity. Since large particles settle down fast during alignment, only the movement of suspended particles was used to measure zeta potential.

Solution depletion method was employed to determine the adsorption of PEI on SiO_2 particles. Polymer concentration in the supernatant was determined by total organic carbon (TOC) analyzer (Tekmar-Dorhman Phoenix 8000) utilizing UV light and persulfate oxidation techniques to break down species containing organic carbon to CO_2, which is then analyzed using a non-dispersive infra-red (NDIR) detector for quantification. First, stock solutions that contained each PEI with different molecular weights were prepared at 1,000 mg/L concentration. 100 ml of each solution at desired concentration was made by gravimetric dilution with DI water from the stock solution. 5 g of silica powder were mixed with the prepared PEI solution in polyethylene bottles. Then, samples were ultrasonicated at the power of 80 W for 3 minutes followed by

shaking for 4 hours in a twist-shaker to reach equilibrium. 4 hour shaking was enough for an equilibrium state in comparison with the result of 24 hour shaking. After equilibrium, 40 ml of the suspension was centrifuged at 10,000 rpm for 10 minutes and supernatant was filtered using a 0.2 μm filter cartridge.

Turbidity measurement is one of the simpler tests to estimate the dispersion of the colloidal suspension. Coagulated particles will settle down faster than the well-dispersed particles and a low turbidity number is expected. Samples for turbidity test were prepared from the same suspensions as used for adsorption test. 50 ml of suspension was decanted to a clear glass bottle and mechanically shaken for 1 minute right before the measurement. Turbidity was recorded utilizing Hach 2100 AN turbidimeter (Hach Co., CO) at the interval of 30 seconds and the data shown here are only after 5 minute settlement. The unit of turbidity is the Nephelometric Turbidity Unit (NTU).

Results

Figure 3-2 shows the zeta potential measurement of silica particles with different molecular weights of PEI. Silica particles have negative charges over the pH range from 3 to 10.5 and the zeta potential increases with pH. As PEI was adsorbed to the silica surfaces, the charges reversed, resulting in a positive zeta potential. Since PEI has more positive charges at lower pH, the zeta potential of PEI adsorbed silica particles increases as pH decreases. IEP of PEI adsorbed silica particles was determined to be about 10, at which point the degree of ionization is small. This result is in good agreement with previous studies [72, 82, 83] and the electrophoretic mobility of PEI [84].

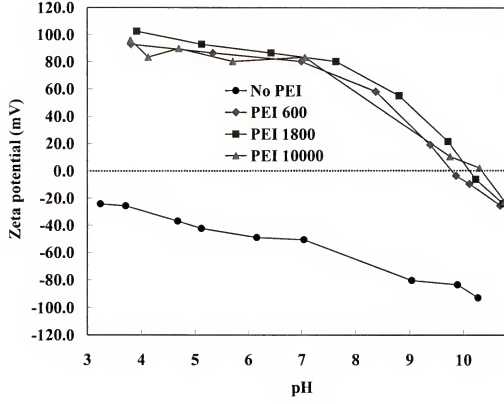

Figure 3-2. Zeta potential of silica particles with or without PEI of different molecular weight PEI as a function of pH in 0.0005 M NaCl.

Adsorption of PEI

Adsorption isotherms of PEI on SiO_2 are presented as a function of pH for different ionic strengths in Figures 3.3-3.4, where the amount of polymer that is adsorbed per unit surface area is plotted against the total amount of PEI that is added to the solution. A dotted line in each graph represents the complete adsorption of polymer. As the concentration of polymer increases, the amount of polymer that is adsorbed increases and it reaches to a plateau region. This polymer adsorption behavior was fitted with the non-linear Langmuir equation, which is expressed as

$$\frac{1}{\Gamma} = \frac{1}{K\Gamma_{max}} \cdot \frac{1}{C} + \frac{1}{\Gamma_{max}} \tag{3-1}$$

where Γ is the amount of solute adsorbed at concentration C, K is the equilibrium constant and Γmax is the maximum adsorbed amount. The maximum adsorption density, Γmax, was estimated from the extrapolation of intercept on the plot of $1/\Gamma$ versus 1/C. As shown in the following figures, the adsorbed amount of PEI is strongly pH dependent. A large amount of PEI was adsorbed at pH 10 corresponding to a high affinity to SiO_2. On the contrary, the isotherms that correspond to pH 3.8 and 6.8 showed a relatively low affinity and resulted in a large amount of polymers remaining free in solution.

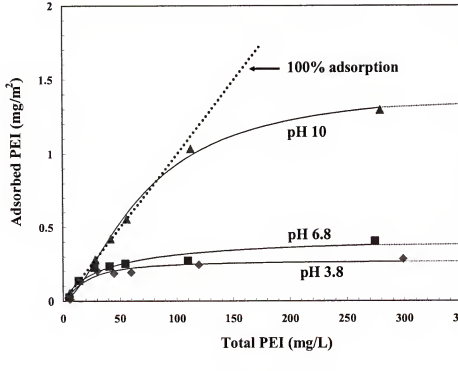

Figure 3-3. Adsorption isotherm for PEI (Mw=10,000) on SiO_2 as a function of pH in $5x10^{-4}$ M NaCl solution. Data was fitted with the Langmuir adsorption isotherm equation (solid line). The dotted line represents the extrapolation from the Langmuir equation.

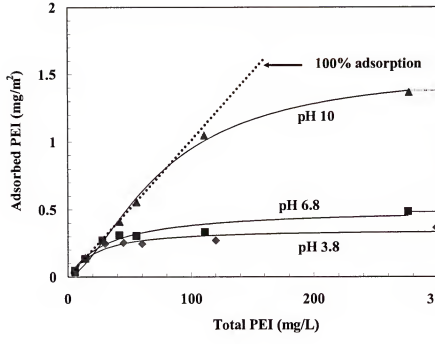

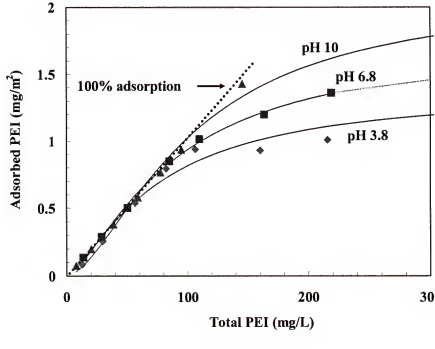

Figure 3-4. Adsorption isotherm for PEI (Mw=10,000) on SiO_2 as a function of pH in NaCl solution (a) $3x10^{-3}$ M, (b) 10^{-2} M. Data was fitted with the Langmuir adsorption isotherm equation (solid line). The dotted line represents the extrapolation from the Langmuir equation.

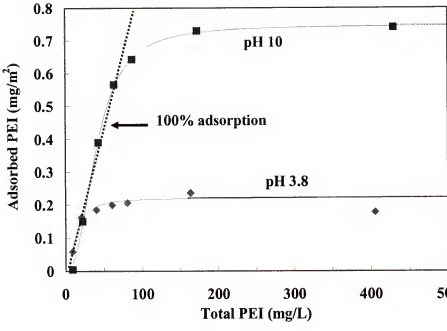

Figure 3-5. Adsorption isotherm for PEI (Mw=600) on SiO_2 in $5x10^{-4}$ M NaCl as a function of pH. Data was fitted with the Langmuir adsorption isotherm equation (solid line). The dotted line represents the extrapolation from the Langmuir equation.

Figure 3-5 and 3-6 represents the adsorption of PEI with Mw 600 and 1,800 at pH 3.8 and 10, respectively. Similar adsorption behavior as that of Mw 10,000 PEI was observed for smaller molecular weight polymers; the higher the pH, the higher the adsorbed amount. For PEI 600, the concentration at which the maximum adsorption of polymer occurs is about 300 mg/L at both pH 3.8 and 10. This indicates that no further adsorption takes place once a complete monolayer of PEI is formed with a low molecular weight polymer. This may be attributed to the fewer possibilities of conformational variations for the low molecular weight polymer in order to adsorb more segments. For low ionic strengths, the adsorbed amount of PEI was saturated with a relatively lower PEI

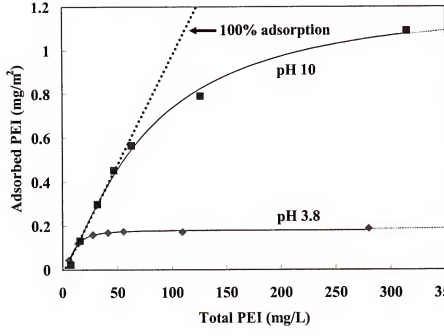

Figure 3-6. Adsorption isotherm for PEI (Mw=1,800) on SiO_2 in $5x10^{-4}$ M NaCl as a function of pH. Data was fitted with the Langmuir adsorption isotherm equation (solid line). The dotted line represents the extrapolation from the Langmuir equation.

concentration at pH 3.8 irrespective of the molecular weight. As the ionic strength increases, the concentration where the saturation of PEI adsorption occurs also increases. These observations suggest that large and coiled structures of polymer have the tendency to change the conformation on the surface allowing the more molecules to be adsorbed.

Turbidity

Figures 3-7, 3-8, and 3-9 show the turbidity measurement results for SiO_2 suspensions at pH 10 with varying concentration of PEI 600, 1,800, and 10,000. The first graphs show the change of turbidity as sedimentation occurs without perturbation. Since turbidity is read in the central region of the glass tube, turbidity sometimes increases

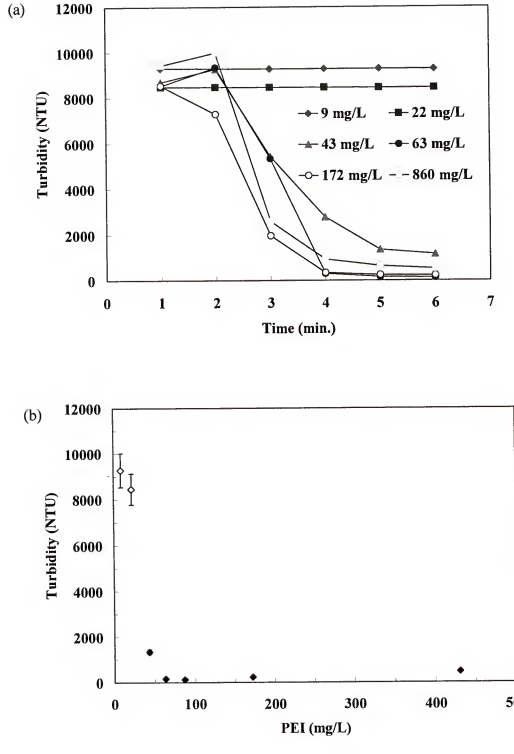

Figure 3-7. Change of turbidity of silica suspension measured at pH 10 and 0.0005 M NaCl (a) with varying the concentration of PEI 600 as a function of time. (b) Turbidity after 5 minute sedimentation.

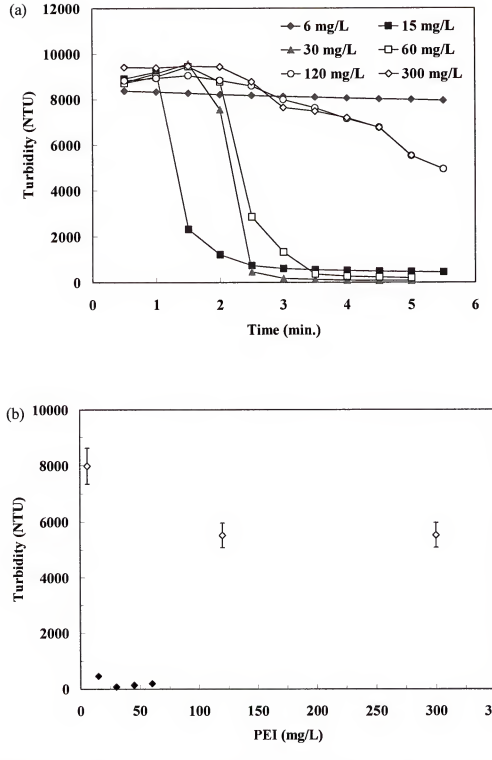

Figure 3-8. Change of turbidity of silica suspension measured at pH 10 and 0.0005 M NaCl (a) with varying the concentration of PEI 1,800 as a function of time. (b) Turbidity measured after 5 minute sedimentation.

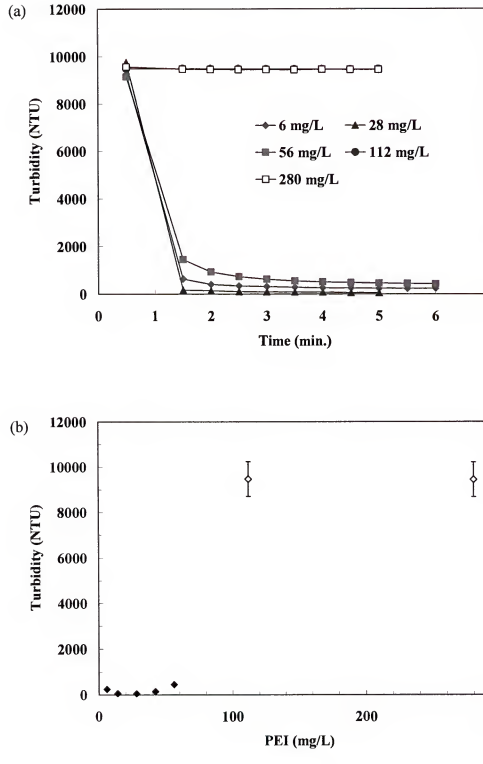

Figure 3-9. Change of turbidity of silica suspension measured at pH 10 and 0.0005 M NaCl (a) with varying the concentration of PEI 10,000 as a function of time. (b) Turbidity measured after 5 minute sedimentation.

around 2 minute settlement due to the increase of particle numbers, which results from the sedimentation of particles in the upper region. From the figures, the sedimentation rate of flocculated suspension increases with the molecular weight of PEI.

The second graphs in each figure is the turbidity after 5 minute sedimentation and the closed and open symbol represent the flocculation and dispersion state of the suspension, respectively. General trend is that turbidity decreases with adding a small amount of PEI for all three molecular weights. Screening of electrostatic charge of the silica surface by the adsorbed polymer with the low concentration induced decrease of zeta potential and flocculation of the suspension. However, while silica particles adsorbed with less than 10 mg/L of PEI 600 and 1,800 were still in a dispersed state, one with 6 mg/L of PEI 10,000 was flocculated. For PEI 10,000, polymer bridging between two particles may be another reason as well as the decrease of electrostatic charge to result in faster settlement of flocculated particles. From Figure 3-3, 3-5 and 3-6, it is seen that the silica surface was mostly covered after adding over 100 mg/L. However, with a large amount of added polymer which is enough to form monolayer of PEI on silica surface, a different dispersion behavior was observed depending on molecular weight. Whereas PEI 600 suspension was still in a flocculation state at high concentration, PEI 1,800 and 10,000 suspensions were re-dispersed.

Discussion

Effect of pH

SiO_2 particles are negatively charged (IEP ~ 2) as seen Figure 3-2 and PEI is positively charged (degree of ionization ~ 80% [81]) at pH 3.8. Thus, one may expect that high adsorption on SiO_2 surfaces may occur because of the electrostatic attraction between the opposite charges of PEI segments and silica surfaces at pH 3.8. However,

low adsorption of PEI observed at this pH is likely attributed to the repulsion between the charged segments of the polymers, which would prevent the polymers from adsorbing on the oppositely charged surfaces. According to the theory of polyelectrolyte adsorption kinetics, attraction between the charged surface and the PEI segment is dominant when the surface is almost empty. However, a barrier against further adsorption is developed with increasing surface coverage by the electrostatic repulsion. This barrier blocks the further adsorption of the charged polymer molecules and the interaction between the polymer molecules becomes more significant.

At pH 6.8, the adsorbed amount increases by decreasing the polymer charge density and increasing the surface charge because the attractive interaction between the surface and charged segments becomes dominant over the repulsive interaction between the segments and segments of the polymer. At pH 10, the ionization degree of PEI is smaller, the segment/segment repulsion weakens further, and higher adsorption is achieved. It should be noted that when segments are in close proximity to the surface, the degree of ionization may vary not only with pH of the solution but also the distance from the oppositely charged surfaces [85, 86]. According to the lattice-based model [87] for polyelectrolyte interactions at solid/liquid interface, the local electrostatic potential near the surface influences the segmental ionization of the polyelectrolyte. This means that the amino groups of PEI in contact with the charged silica are more charged than degree of protonation in bulk solution and ones further from the surface are less charged. Segments can adjust its ionization to compensate the charge of the surface and this localized charge compensation of the polymer adsorbed to the surface may change the Stern potential even at high pH, where the polyelectrolytes are almost neutral in solution. Despite of this

induced adsorption by localized charge compensation, because there is a small electrostatic attraction between the polymer and surface, it is not sufficient to say that only the decrease of electrostatic repulsion between the segments leads to the larger adsorbed amounts at pH 10. This implies that in addition to the decrease of segment/segment repulsion, there must be strong affinity of PEI to silica surface of nonelectrostatic origin because polymer adsorption by localized electrostatic attraction may be prevented by the screening of the small counter-ions at high pH.

Not only the electrostatic adsorption barrier of polymer, but also the rearrangement or the conformational change of the adsorbed polymers is responsible for the adsorbed amount. PEI is has a coiled or folded structure at high pH and undergoes transitions from a coiled conformation to a stretched one at low pH due to the repulsion between the charged segments of the molecules. These unfolded polymers may be adsorbed in a flattening form occupying the larger adsorption sites available on the SiO_2. However, it should be also considered that the standing structure of the stretched polyelectrolyte on the solid surfaces, if there is competition between the molecules to locate the adsorption site. On the other hand, the larger adsorbed amounts are achieved at a high pH because the occupied spaces are small due to more compact size of the coiled polymer.

Effect of Ionic Strength

Ionic strength of the suspension is another factor impacting the adsorption of polyelectrolytes on charged surfaces. For Mw 10,000 PEI, all solubilized polymer adsorbs completely for less than 100 mg/L in solutions with 0.5 mM and 3 mM NaCl; whereas about 150 mg/L is necessary for 10 mM solution. Figure 3-10 gives the maximum amount of the adsorbed PEI to silica powders versus pH and sodium chloride concentration. As shown in the figures, the higher adsorption capability was observed for

higher ionic strength. This may attribute to the screening of the PEI charges by the counter-ions reducing the repulsive interaction between the segments. Ionic strength effect on the adsorption is more significant at low pH. This indicates that a significant nonelectrostatic affinity of PEI to silica exists. By screening the electrostatic interactions with ionic concentration, nonelectrostatic affinity of PEI to the silica surfaces becomes dominant and adsorbed amount increases, so called, screening enhanced adsorption [88]. Ionic strength effect decreases with increasing pH since the attractive interaction between the segments and surface becomes more pronounced than the repulsive segment/segment interaction. This also implies that there must be a pH where the adsorption does not depend on the ionic strength. From Figure 3-10, it is expected that the amount of maximum adsorption could be same at about pH 12 irrespective of ionic strength. Above pH 12, where PEI behaves like a neutral polymer, adsorption of PEI might decrease with increasing ionic strength, which is called screening reduced adsorption [88]. According to the model of Van de Steeg et al. [88], there is a transition region between the screening enhanced and reduced adsorption of polyelectrolyte depending on the charge density of segment and surface and on the nonelectrostatic affinity of the polyelectrolyte toward the surface.

Effect of Molecular Weight

As shown in Figure 3-2, at high pH above 10.5 where PEI is not ionized, the charge reversal of silica did not take place and the zeta potential decreased as the molecular weight increased. These behaviors are most likely caused by two reasons, which are definitely dependent on the molecular weight. First, local ionization of polymers near surfaces partially screens the charge on the particles, subsequently decreasing the zeta

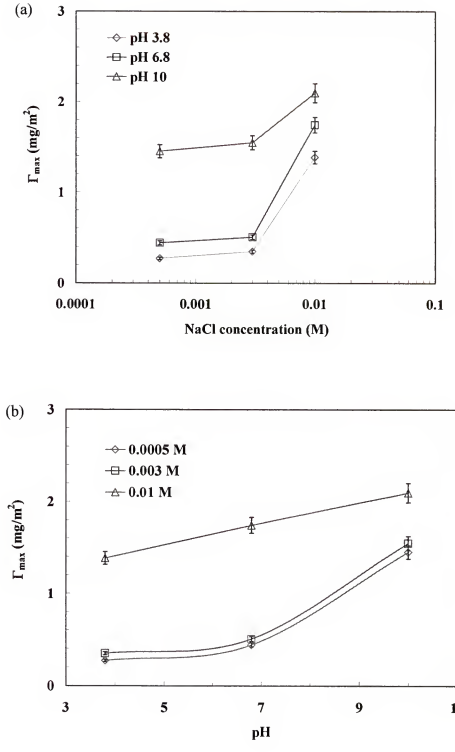

Figure 3-10. The amount of maximum adsorption of PEI (Mw=10,000) on SiO_2 powder in solutions with (a) different NaCl concentrations at different pH values. (b) redrawing as a function of pH varying NaCl concentration.

potential. Second, the shear plane might be displaced further out from the particle surface by the presence of the polymer chains.

The effect of molecular weight on the adsorption of PEI to silica surfaces is shown in Figure 3-11. Adsorption density increased linearly as the logarithm of molecular weight increased at pH 10 but was almost independent of the molecular weight at pH 3.8. This behavior suggests that, at low pH where polymers are mostly ionized, adsorption of PEI is dominated by the electrostatic interaction between the charged polymer molecules and surface charges of particle surfaces. However, in non-ionized condition, adsorption of PEI is pretty dependent on the molecular weight and this implies that the interactions between polymer molecule segments and particle surface are dominated by other types of interactions which are dependent on the chain length such as hydrogen bonding or hydrophobic attraction force.

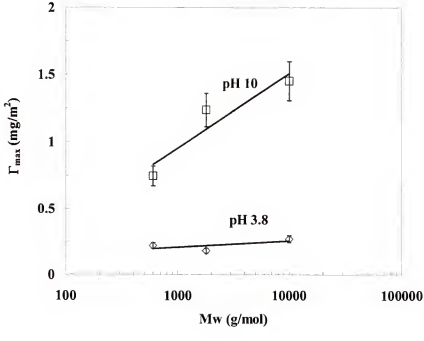

Figure 3-11. A logarithmic plot of maximum adsorption of PEI (Γ_{max}) on SiO_2 as a function of molecular weight at pH 3.8 and 10.

The turbidity of the silica suspension as a function of the concentration of PEI 600 is shown in Figure 3-12 by superimposing the adsorption isotherm at pH 3.8 and 10. For comparison, the adsorption isotherm and the turbidity of the silica with PEI 10,000 at pH 3.8 and 10 are also represented in Figure 3-13. Here is indicating that stability of colloidal suspension with polyelectrolytes is determined by both the electrostatic charges and the polymer conformation developed on the particle surfaces. Since electrostatic charges of PEI-adsorbed silica are small at pH 10 (see Figure 3-2) for both Mw, conformation of PEI, i.e., repulsive layer thickness is more critical factor in dispersion of the particles.

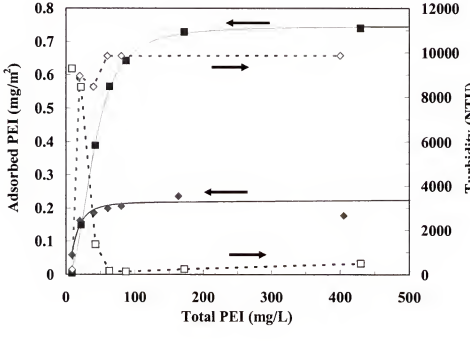

Figure 3-12. Adsorption isotherm and turbidity of SiO_2 suspension with PEI 600 as a function of total amount added in 0.5 mM NaCl solution. Diamond and square symbol denotes the pH 3.8 and 10, respectively.

As seen in Figure 3-12, the dispersion behavior is not simply determined by the adsorbed amount of polyelectrolyte. Even though a larger adsorbed amount of PEI was attained at pH 10 than pH 3.8, the better dispersion was achieved at pH 3.8. Since the repulsive layer thickness formed by PEI 600 at pH 10 was not enough to overcome the attractive vdW forces, the re-dispersion of the suspension did not take place even above the certain concentration where the complete surface coverage of PEI occurred. Unlikely to the suspension at pH 10, a stable silica suspension was achieved with forming a monolayer of PEI 600 at pH 3.8. This may be due to the standing structure of the unfolded molecules, which makes the PEI layers be thick enough to overcome the vdW force or the electrostatic repulsive forces between positively charged polymers adsorbed to silica. Only from the adsorption isotherm data, it cannot be concluded what conformation of PEI is formed on the silica surfaces at low pH.

For PEI 10,000, the adsorbed amount and state of dispersion of silica particles matched well irrespective of pH. In other words, the dispersion was determined by the adsorption amount with high Mw polymer at any pH through the electrostatic and/or steric stabilization mechanism. Inset in the figure represents the turbidity of the silica suspension at pH 10 with the PEI concentration below 100 % adsorption. At high pH, polymer bridging may exist below 100 mg/L concentration due to incomplete coverage of the silica surface. As seen in the figure, complete surface coverage was achieved at about 60 mg/L and polymer bridging effect must be a maximum when 50% of each surface is covered which is corresponding to the minimum turbidity at 30 mg/L.

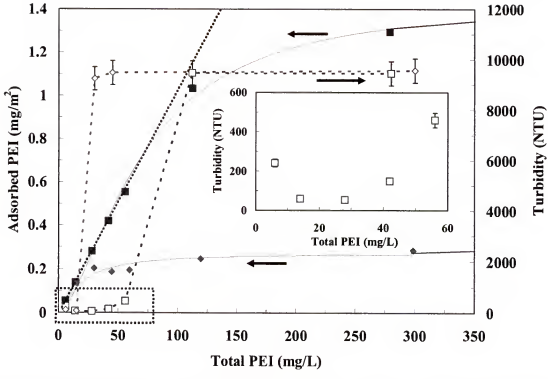

Figure 3-13. Adsorption isotherm and turbidity of SiO_2 suspension with PEI 10,000 as a function of total amount added in 0.5 mM NaCl solution. Diamond and square symbol denotes the pH 3.8 and 10, respectively.

Summary

Adsorption of PEI on the silica particles was studied as a function of pH, ionic strength, and molecular weight. The zeta potential of the silica particle was reversed with the adsorption of PEI due to positive charges on the chains. General feature of the adsorption of PEI on silica surfaces is that as pH and ionic strength increased, the adsorption density increased for all molecular weight PEI solutions. Whereas an electrostatic repulsive interaction between the positively charged segments is dominant at low pH, nonelectrostatic interactions between the segments and silica surface become important at high pH. The ionic strength effect is more significant at low pH due to the screening of repulsion between the charged segments. The maximum adsorption amount

is independent of the molecular weight of PEI at low pH but increases linearly with the logarithm of the molecular weight. This also suggests that PEI adsorption at high pH is controlled by other interaction forces than electric double layer force.

Since the adsorbed amount and the conformation of PEI are dependent on pH value, the stability of the silica suspension is affected by the molecular weight, i.e. layer thickness of the adsorbed PEI. While silica particles were flocculated with PEI 600 at pH 10, the ones with PEI 1,800 and 10,000 are well dispersed after forming the monolayer of PEI at the same pH. However, well dispersed silica suspensions can be achieved with PEI 600 at a low pH by either a thick layer formation or EDL repulsion. The surface force measurement in the next chapter will elucidate the mechanism of the dispersion.

CHAPTER 4
SURFACE FORCES BETWEEN PEI LAYERS ADSORBED TO SILICA SURFACES

Introduction

In chapter 3, the electrokinetic behavior and dispersion of silica particles adsorbed with PEI have been discussed. Polyelectrolyte has not only the electrostatic property but also polymeric nature, which cannot be evaluated with the zeta potential measurement. For example, zeta potentials of silica suspensions with different molecular weight are of similar low values at pH 10, the dispersion behavior of the suspension is quite different. While PEI 600 showed flocculation of particles, well dispersed silica suspensions were attained with PEI 1,800 and 10,000. Turbidity or viscosity measurement is an efficient technique to compare the relative dispersion state of suspensions, but falls short of understanding the interaction behavior between individual particles. For example, some forces such as structural or hydration force can be validated clearly with the direct surface force measurement. Combined with the other techniques, surface force measurement allows us to obtain more detailed information on the colloidal behavior of the suspension.

Surface force measurements in the liquid environment were first performed with SFA by Israelachvili and Adams in 1976 [89]. Since then, there have been many studies on surface forces between polymer layers adsorbed or anchored to surfaces such as interaction force between polystyrenes adsorbed on mica surfaces in cyclohexane [90, 91]. However, because samples for SFA are required to be transparent due to multiple beam interferrometry, which measures the separation distance, the interaction force study is limited to a few of materials such as mica or glasses. Currently, further development has

been made such as a new bimorph SFA method, which is called a Measurement and Analysis of Surface Interaction Forces (MASIF) for extending the capability of SFA to measure opaque materials [92]. On the other hand, because of the higher force sensitivity and availability of various samples, AFM colloidal probe technique has been widely used for surface force measurement. There are numerous surface force studies using colloidal probe in polymer or polyelectrolyte solution such as interaction between polyacrylic acid (PAA) layers adsorbed on zirconia [93] or silicon nitride [94], polyethylene oxide (PEO) on glass surfaces [95]. Claesseon et al. [73] studied the interaction between PEI layers on mica surfaces as a function of amount of PEI at two ionic strengths without adjusting pH. Their major finding is that while zeta potential determined by electro-osmotic mobility was consistent with the interfacial potential deduced from the force measurement for flat layer of PEI, it was significantly less than interfacial potential for a thicker layer due to the increase of tail fraction of PEI for coiled structures. Similarly, Poptoshev et al. [96] studied the interaction between PEI layers on flame polished glasses and compared with linear polyvinylamine (PVAm). By comparing similar molecular weight PEI and PVAm, they claimed that PEI has a higher charge overcompensation and shorter separation distance where polymer bridging occurs. This is due to the branching of PEI which leads to higher number of charges and smaller contour length. However, the systematic study on the interaction of PEI layers adsorbed on silica surfaces as a function of pH, ionic strength, and molecular weight has not been done yet by correlating adsorption and dispersion.

Experimental

Materials

Micrometer sized silica spheres were purchased from Duke Scientific Corp. and have and RMS roughness of less than 0.2 nm. Spheres were cleaned with ethanol and DI water one after another several times and dried in a vacuum oven for several hours. A plasma enhanced chemical vapor deposited (PE-CVD) SiO_2 coating on a silicon wafer supplied by Motorola was used as a substrate. 2 μm thickness of SiO_2 layer and 0.3 nm RMS roughness was determined by Ellipsometry and AFM. The silica surface was cleaned by ultrasonicating with the order of detergent, acetone, and ethanol for 30 minutes respectively, rinsed with DI water and dried with air blow prior to use. 200 mg of polyethyleneimines (PEI, 99 %, Alfa Aesar, MA), with average molecular weights (Mw) of 600, 1,800, and 10,000 g/mol without further purification were mixed with 100 ml of sodium chloride solution and stirred for 2 hours for complete dissolution. The pH of the suspension was adjusted with ACS reagent grade hydrochloric acid (HCl) and sodium hydroxide (NaOH). Radius of gyration (R_g) and Flory radius (R_F) for different molecular weight PEI were calculated by the Equation 2-35 and 2-39 shown in Table 4-1.

Table 4-1. Calculated Flory radius, R_F and radius of gyration, R_g for different Mw PEIs. Polymer is assumed to be linear and length of monomer is 0.38 nm. Dimensionless excluded volume parameter is 0.6.

Molecular weight (g/mol)	Flory radius R_F (nm)	Radius of gyration R_g (nm)
600	1.847538	1.419466
1,800	3.571626	2.458587
10,000	9.993153	5.794946

Method

Two types of cantilevers were purchased from Digital Instrument and surface forces were measured with a commercial multimode atomic force microscope (AFM) (Nanoscope III, Digital Instrument, CA). A contact mode triangular Si_3N_4 cantilever was used for attaching microsphere according to the method developed by Ducker et al. [61]. Single silica microsphere whose radius is about 25 μm was glued with a low melting temperature resin (Epon R 1004, Shell Chemicals Co.) on the cantilever by using a glass fiber with 10 μm diameter under the optical microscope. The assembled cantilever was heated on a hot plate and checked if the sphere was located at the end of the cantilever. It was washed again with ethanol and ultrapure water prior to the force measurement in order to remove the possible contamination on the surface during the attachment of the particle. A contact mode Si cantilever was also used for investigating interaction forces of the bare AFM tip. Spring constants of cantilevers were measured by the Cleveland method [67] yielding 0.26 N/m (±0.03) for Si_3N_4 tips and 0.05 N/m (±0.02) for Si tips.

All measurements were done in a fused silica liquid cell where the cantilever was designed to submerge completely. The advantage of the operation in the liquid cell is that capillary adhesion induced by a liquid meniscus between the probe and sample can be negligible [97]. After the cantilever and substrate were installed in the AFM, 20 ml of the PEI solutions were injected through the silicone tubing and allowed 15 minutes for PEI molecules to adsorb on the silica surfaces. Then 20 ml of bulk solutions with the same pH and ionic strength were injected to remove the effect of non-adsorbed polymer molecules in the precedent solution and equilibrated for 10 minutes. Force measurements were conducted on three different positions of the silica substrates with at least five

measurements at each position by a Z-scan rate of 0.5 Hz and a scan size of 600-1000 nm, which corresponds to an approaching velocity in the range of 300-500 nm/s. The force-separation plot was converted from each deflection signal – piezo scanner movement data and averaged with the data analysis software.

Results and Discussion

Interaction Forces between Bare Silica Surfaces

Figure 4-1 shows the typical AFM colloidal probe and AFM image of PECVD SiO_2 substrate taken before the force measurement. Diameter of single silica sphere was 46.2 μm and RMS roughness of the SiO_2 substrate was 0.032 nm.

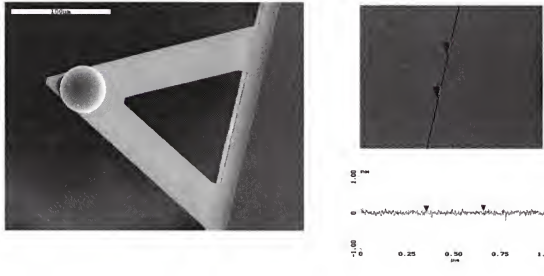

(a) (b)

Figure 4-1. Materials used for surface force measurement. (a) SEM image of a spherical SiO_2 particle attached on the tipless triangular contact mode Si_3N_4 AFM cantilever and diameter of the sphere is 46.2 μm. (b) AFM image of PECVD SiO_2 substrate and RMS roughness is 0.032 nm

Figure 4-2 shows normalized force-separation curves between the silica sphere and plate without any PEI in pure electrolyte solution at pH 4 and 10. When they come close to about 70 nm of separation distance, the electrical double layer developed on the surface started to overlap. Since silica surfaces are negatively charged down to about pH 2, the repulsive interaction force took place for both pH 4 and 10 and the interaction force is smaller for lower pH because of the lower surface charges of silica. Although both curves fitted well to the DLVO theory at a large separation with a decay length of 30 nm, interaction force behaviors at short separation were a little bit different. A large repulsion instead of primary minimum occurred at separations below 4 nm at pH 10 and this extraordinary repulsive force at short separation distance in aqueous media cannot be explained by the conventional DLVO theory. The non-DLVO repulsive force has been reported with various types of glass or silica surfaces [98-101] and two hypotheses have been proposed, one of which is the hydration repulsive force. Because of the structuring of water molecules and/or hydrated ions adsorbed at the silica surface resulting in an increase of free energy, a short range repulsive force, so called, hydration repulsion may occur when silica surfaces approach each other. Since the ionic strength in the solution is the same for both solutions, if the non DLVO repulsive force originated from the hydration repulsion, this force also must have been observed at pH 4. However, even though the measured force deviated from the DLVO model at a separation of 8 nm, the repulsive force was not as obvious as that for pH 10. This may be due to the lesser affinity of the hydrated ions to the silica surfaces at low pH due to the lower surface charge, resulting in a loosely structured layer.

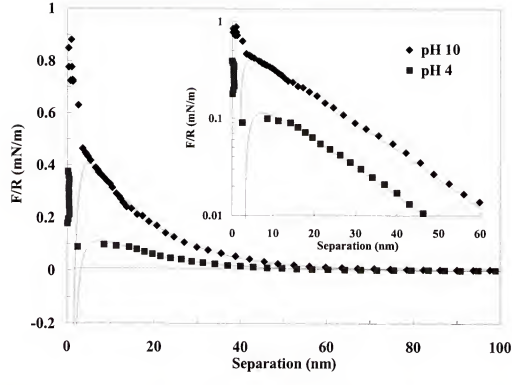

Figure 4-2. Normalized force-separation profile plot between silica probe and silica substrate in $4x10^{-4}$ M NaCl solution. Data were fitted with the non-linear DLVO theory with a constant charge boundary condition with a Stern potential of -32 mV for pH 10, and -19 mV for pH 4. Hamaker constant for non-retarded vdW force was $1.2x10^{-20}$ J.

The second mechanism of non DLVO repulsive force proposes that water molecules may diffuse in the silica surface by breaking siloxane bonds (Si-O-Si) and forming hydroxylated surfaces. Some bonds of these structures may also break and form silicic acid chains inducing a gel-like layer structure and the short range repulsive forces are attributed to the steric origin of silicic acid chains in the layer. According to Alexander [102], the formation of gel layer is easy to occur at higher pH because hydroxyl groups in solution accelerate the reaction between water and siloxane bonds. Even though a relative fast reaction between them has recently been suggested in mid pH

regime [101], a small repulsive force at pH 4 suggests that a thinner gel layer may be formed or does not exist at this pH during the time period (less than 1 hour) of our experiment.

The normalized interaction forces between silica sphere and plate in different ionic strength solutions at pH 10 are represented in Figure 4-3. Because of the EDL repulsion between negatively charged silica surfaces, repulsive forces were observed for 0.4 mM and 10 mM NaCl concentration. Repulsive forces decreased as ionic strength increased due to the compression of EDL as expected. With the highest ionic strength (0.1 M), there was a mere contribution from the EDL repulsion and attractive vdW force became responsible for the total interaction force. The magnitude of attractive force of 0.1 M solution was smaller than that expected from the DLVO theory. This may be due to the ionic screening of the surface, changing the Hamaker constant. Non-DLVO repulsive forces were observed for all three electrolyte solutions. Even for 0.1 M solution, the repulsive force was observed at 2 nm of separation distance.

Figure 4-3 (b) gives the force profile for silica surfaces being separated from each other. Inset in the figure shows the maximum adhesion as a function of ionic strength, which was calculated from subtracting minimum force in Figure 4-3 (b) from maximum repulsion in Figure 4-3 (a). The adhesive force decreased with increasing electrolyte concentration. In addition, as the ionic strength increased, the separation range, where the minimum adhesion occurred at, increased. This suggests the formation of a thicker structured layer, which is composed of water molecules, ions and hydrated ions on the surface when the more salt ions are adhered to the surface of particles. According to Malkina and Vakaleski [103], the strength of adhesion is dependent on how far the

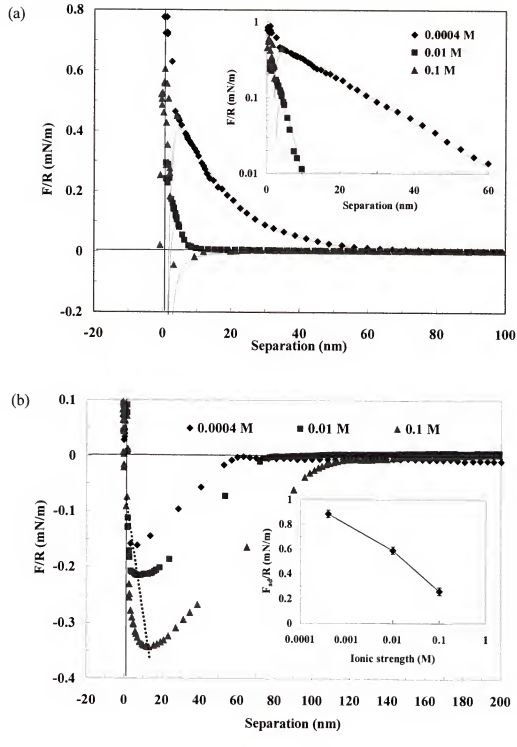

Figure 4-3. Normalized force-separation profile between silica probe and silica substrate with varing NaCl concentration at pH 10. Data were fitted with the non-linear DLVO theory with a constant charge boundary condition with a Stern potential of -32 mV for 0.4 mM, -16 mV for 10 mM, and -5 mV for 0.1 M. Hamaker constant for non-retarded vdW force was 1.2×10^{-20} J.

particle can penetrate into the adsorbed layer during contact. Arguments still exist about the origin of short-range repulsive forces of silica surfaces, such as the dependence on the history of synthesis of silica particles and heat treatment of sample. However, once the polymers or polyelectrolytes are adsorbed on the solid surfaces, the total interaction behaviors of the colloidal particles are decided by their concentration and properties such as conformation and charge density, etc.

Interaction Forces between PEI Layers Adsorbed to Silica Microsphere and Substrate

Figure 4-4 shows the force measurement of silica surfaces with varying concentration of PEI 1,800 in pure water without adding any intentional salt. Retracting force curves for all the concentrations are the same as those of approaching curves and no hysteresis was observed. Interaction force at large separation distances decreased as the concentration of PEI increased. At pH 10, the electrostatic component induced from the PEI is considered to be small due to low ionization and most EDL force comes from the surface charges of silica. As expected in the adsorption isotherm of PEI, a small amount of PEI would be adsorbed in low electrolyte concentration until the maximum saturation of PEI occurred. As the PEI concentration increases, the more locally charged PEI segments screen the charge on the silica surface and induce the decreased EDL forces. However, the adsorbed amount increases, the more tails exist and the layer thickness will increase. Therefore, the steric interaction occurred at separation of about 4 nm for 200 mg/L of PEI and 10 nm for 2,000 mg/L of PEI. Even though barely seen in the figure, a higher repulsive force was observed between 2 and 4 nm of separation distance as PEI concentration increases and the force magnitude was almost same irrespective of

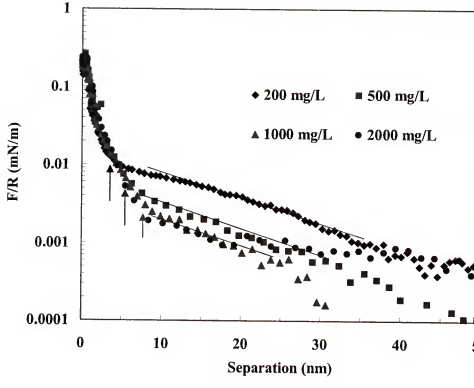

Figure 4-4. Interaction forces between silica surfaces with different amount of PEI (Mw=1,800) at pH 10 in pure water. Solid line denotes the electrostatic repulsive force.

concentration below 2 nm. This suggests that a quite dense or incompressible polymer layer of about 1 nm thickness is formed.

Figure 4-5 is the interaction force measured with PEI 600 in 0.5 mM NaCl solution. For pH 10, although a small repulsive force was found in the range between 25 nm and 40 nm, the attractive force was dominant at a shorter separation distance due to vdW force. At a separation of 4 nm, another steep repulsive force was observed, which may from the repulsion between the adsorbed PEI layers. Considering the radius of gyration of linear PEI 600 as 1.4 nm, 1 nm of R_g for branched PEI 600 is in the reasonable range at pH 10. On the other hand, the repulsive force started to occur at 40 nm of separation

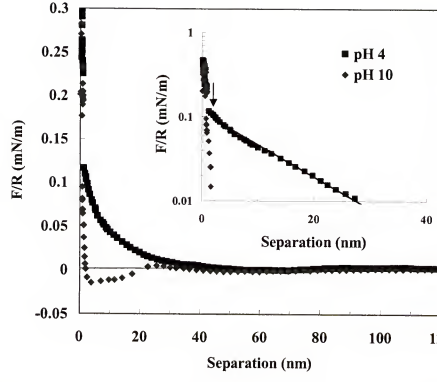

Figure 4-5. Normalized force-separation profile between silica probe and silica substrate with PEI 600 at different pH in $5x10^{-4}$ M NaCl concentration.

distance at pH 4, which is the similar interaction range as that of pH 10. However, the repulsive force kept increasing as the opposing surfaces come closer. Surface force measurements at different pH values are consistent well with the zeta potential and turbidity results in that silica suspension with PEI 600 flocculated at pH 10 and dispersed at pH 4. From the logarithmic plot in the inset, the repulsive force at pH 4 follows the non-linear PB equation up to 2 nm of separation distance, which indicates that the interaction between PEI 600 layers are of electrostatic origin. Below the 2 nm, the existence of the PEI layer is responsible for the repulsive interaction. This indicates that thinner PEI layers are formed at a low pH by covering silica surfaces in a flatter conformation than pH 10.

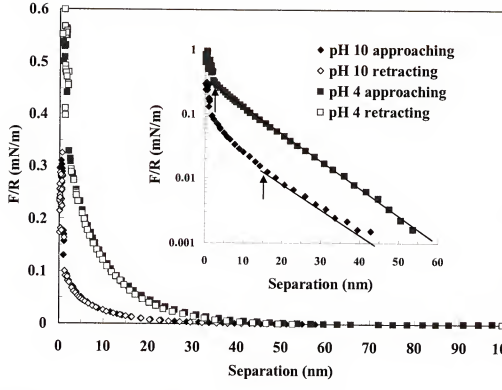

Figure 4-6. Normalized interaction forces between silica sphere and silica plate surface with adsorption in 2,000 mg/L of PEI solution (Mw=10,000) at pH 4 and 10 in $3x10^{-3}$ M NaCl. Solid line denotes the Debye length.

Figure 4-6 represents the interaction force of PEI 10,000 adsorbed layers on silica sphere and plate at pH 4 and 10. Same interaction force-separation plot was observed when the probe was retracted from the substrate without any hysteresis. As seen in the figure, the repulsive force was observed for both pH values occurring at about separation of 45 nm. At a larger separation, electrostatic force is dominant. However, the steric force starts to interact at about separation of 15 nm for pH 10 and 4 nm for pH 4 solutions. As mentioned in the above, this indicates that the thicker PEI layer was developed at pH 10 because PEI molecules are of the folded or coiled structure at a high pH. The stretched structure of PEI at pH 4 causes the flattened conformation of molecules by the

electrostatic attraction between PEI and silica surface. This is also consistent with that the adsorption amount of PEI at a low pH is less than high pH. Because flat conformation of PEI at low pH occupies the larger space for adsorption, a small amount of PEI is absorbed. A total interaction force between PEI layers is larger at pH 4 due to electrostatic repulsion between charged segments.

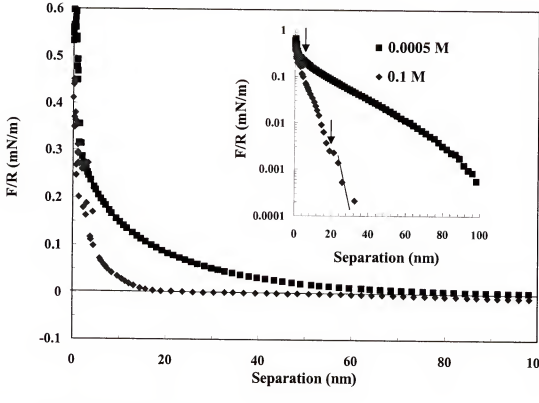

Figure 4-7. Normalized interaction forces between silica sphere and silica plate surface with adsorption in 2,000 mg/L of PEI solution (Mw=10,000) at pH 4 as a function of ionic strength. Solid line denotes the Debye length.

Figure 4-7 represents the effect of ionic strength on the interaction force between PEI adsorbed silica surfaces at low pH. The solid line in the inset represents the Debye length. As shown in figure, the range of repulsive force decreased significantly from a separation of 80 nm to 20 nm. This large decrease of repulsion results from the

compression of electrostatic double layer developed on the PEI layers. For pH 0.5 mM NaCl solution, electrostatic repulsion exists from separation of about 80 nm down to 4 nm. However, for 0.1 M solution, the contribution from the electrostatic force vanishes quickly due to high ionic strength and steric component of polyelectrolyte becomes dominant at separation of 20 nm. This indicates that the flattened conformation of PEI with low ionic strength changes into more folded and standing conformation as ionic strength increases because counter-ions screens the charges of the silica surface as well as the segments of PEI. This is consistent with that the dramatic change of adsorbed amount of PEI at low pH with increasing salt concentration.

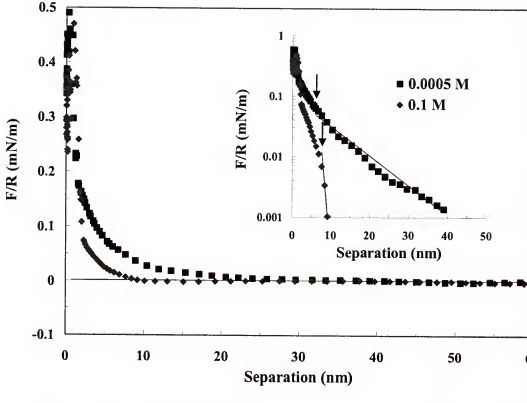

Figure 4-8. Normalized interaction forces between silica sphere and silica plate surface with adsorption in 2,000 mg/L of PEI solution (Mw=1,800) at pH 10 as a function of ionic strength. Solid line denotes the Debye length.

Similar effect of ionic strength on the surface force was observed with PEI 1,800 at pH 10 as represented in Figure 4-8. Because of the lower electrical charge at pH 10, the interaction range is about 30 nm for 0.5 mM and the magnitude at the same separation is smaller than those of pH 4. For 0.1 M solution, the steric repulsive force becomes dominant at separation of about 8 nm. It is noticeable that even though the size of the PEI 1,800 is smaller than PEI 10,000, the separation distance below which interaction between molecules becomes significant is relatively larger, i.e. about 8 nm. This suggests that the PEI layer thickness increases with the ionic strength because of the higher adsorption density of PEI at high pH, which results in the more packed adsorption of PEI molecules.

The possible PEI conformation depending on the pH and ionic strength is schematically suggested in Figure 4-9 with the adsorption isotherm and force measurement. It is well known that PEI is positively charged at a low pH and subsequently has a stretched structure due to the repulsion between segments. This stretched structure occupies a larger area for adsorption at a low pH, which was confirmed with the adsorption isotherm. This indicates that the conformation of charged polyelectrolyte has an expanded form at a low pH and a low ionic strength. However, if the ionic strength increases, these expanded polyelectrolytes are made of a slight coiled structure or straightened up toward the solution from the surface. Another possibility for PEI to adsorb in a stretched form is that PEI molecules might tend to stand up by anchoring one segment to the silica surfaces and diffusing out the other segments. However, it can be concluded that the adsorbed PEI at a low pH has a flattened conformation on silica surfaces because of the much thinner layer thickness than the

radius of gyration of PEI. However, the folded structure of PEI at a high pH results in a higher adsorption density and the thicker layer than at a low pH. Because the ionic strength effect on the adsorption density is not significant at high pH, the interaction range of steric repulsion between PEI layers is not affected by ionic strength as well.

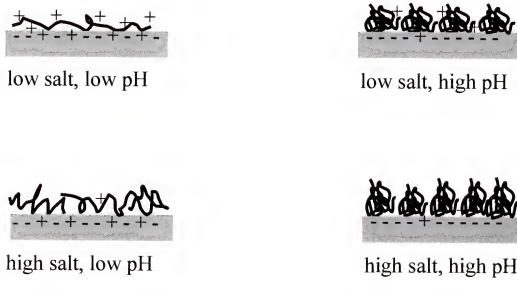

Figure 4-9. A proposed model of different conformation of PEI adsorbed on silica surfaces with varying pH and ionic strength.

Interaction Forces between PEI Layers Adsorbed to Si tip and Silica Substrate

The effects of both pH and ionic strength on the interaction forces between Si AFM tip and silica substrate are shown in Figure 4-10. At pH 10, the range where polymeric interaction occurs is about 12 nm for both low and high ionic strength solution. At pH 4, this interaction range is about 8 nm for 0.0005 M NaCl solution and about 12 nm for 0.1 M NaCl solution. The difference of the interaction range between low and high pH is greater in the lower ionic strength solution as shown in the interaction of microsphere. Since the electrostatic contribution to the repulsion is small for high ionic strength, the

interaction occurring at a separation of about 14 nm attributes to the steric repulsion irrespective of pH of the solution. In comparison with the adsorption isotherm in the previous chapter, although adsorption increases with the ionic strength, the higher adsorption is achieved at pH 10 than pH 4, it can be concluded that more stand-up conformation of PEI at low pH in high ionic strength solution.

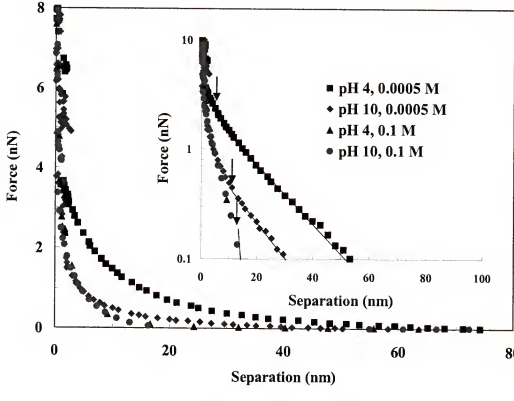

Figure 4-10. Force-separation profile between Si tip and silica substrate with PEI 1,800 at different pH and NaCl concentration. Solid line denotes the Debye length.

Figure 4-11 is the force-separation plot of Si tip with the silica substrate at pH 10 in $5x10^{-4}$ M NaCl solution for different molecular weight PEI. Similarly to the surface force of silica sphere in PEI 600 solution, the attractive force was observed at 15 nm of the separation distance and maximum attractive force is about 0.15 nN at 2 nm of separation.

As Si tip approaches further close to the substrate, small repulsive force occurred due to the repulsion between dense PEI layers. Repulsive forces were observed for PEI 1,800 and 10,000 solutions at pH 10. From the logarithmic plot in the figure, the electrostatic repulsive forces are dominant from 40 nm to 10 nm of separation and polymeric repulsive forces take over the interaction below 10 nm.

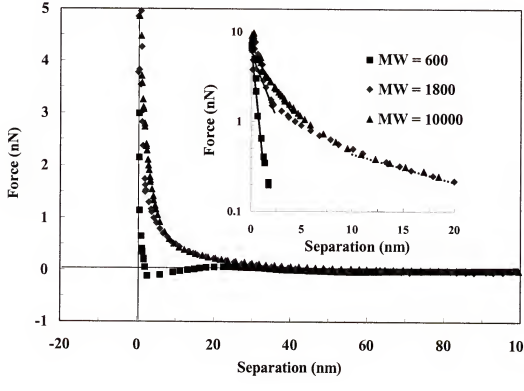

Figure 4-11. Force-separation profile between Si tip and silica substrate with different molecular weight PEI at pH 10 in $5x10^{-4}$ M NaCl concentration. Dotted line is the Debye length. Solid line is for guidance to eye.

One interesting feature is that surfaces forces of silica particles with PEI 600 and 1,800 are dramatically different even with a small discrepancy of molecular weight. The radii of gyration for two polymers are 1.42 nm and 2.45 nm, respectively. This may

suggest that different polymer conformations on the solid surfaces are responsible for the dispersion of nanoparticles not by simply comparing the radius of gyration. The significant difference between two polymers was also observed in rheological behavior of nanoparticle slurries [104]. Dietrich reported that the viscosity of 25 vol% slurry of 100 nm silica particles with PEI 1,800 is about 100 times lower than that of counterpart with PEI 600 and this effect was bigger for 20 nm particles. Considering the radii of gyration of PEI 1,800 and 10,000, 10 nm of polymeric interaction range is relatively small for PEI 10,000. This indicates the PEI layer adsorbed on the very end of the tip, whose radius is of nanometer, may not interact with the loose PEI layer structure on the opposing silica substrate.

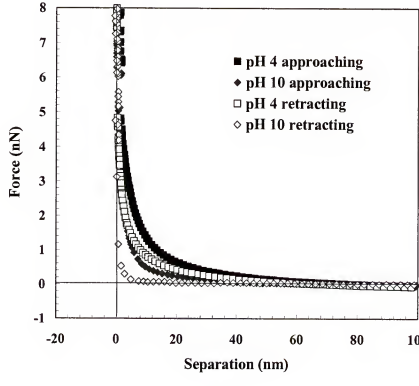

Figure 4-12. Force-separation profile between Si tip and silica substrate with PEI 10,000 at different pH in $5x10^{-4}$ M NaCl concentration.

The interaction force between a bare Si tip and silica substrate in PEI solutions is shown in Figure 4-12. Unlikely to the micrometer sized silica probe, hysteresis of approaching and retracting force curve was observed for both pH solutions. This implies the non-elastic deformation of PEI layers when used the Si tip for a force measurement. It may attribute to another interaction between the side of the tip and substrate. While the PEI layer adsorbed on the end of the tip compresses the PEI layer adsorbed on the substrate at very close separation distance; some PEI molecules on the side of the tip cannot compress elastically the opposite layer.

Summary

The interaction force between PEI layers adsorbed on micron-meter sized silica surfaces as a function of pH, ionic strength, and molecular weight. Comparing the force measurement with the adsorption isotherm and turbidity, the effects of pH and ionic strength on the conformation of PEI layers at silica/water interface and consequently on the interaction force was elucidated. The folded configuration of PEI at a high pH and ionic strength, adsorption amount increases and layer thickness is large. However, folded PEI layers have less electrostatic force at longer separation distance and total repulsive interaction decreases as ionic strength increases. At a low pH, PEI gets unfolded and stretched by the repulsion between the positively charged segments. These charged PEI would have a rather flat conformation on the negatively charged silica surfaces showing the thin steric layer. The majority of repulsive forces of PEI layers adsorbed on silica at a high pH come from the EDL repulsion. The force dependence for Si tips with nanometer radius on pH and ionic strength variation is similar to that of microspheres. However, it is doubtful that AFM tips are useful to represent the behavior of true nanosized particles

because of the geometry of the tip, which may have an influence of the force measurement.

CHAPTER 5
SURFACE FORCE MEASUREMENT USING NANO COLLOIDAL PROBE TECHNIQUE

Introduction

In a previous chapter, interaction forces of micrometer-sized silica particle and bare Si tip in presence of PEI with varying several processing parameters such as pH and ionic strength were discussed. As addressed in previous chapters, the existing force theories have mainly been developed based on relatively large particles from a few hundred nanometers to a few micrometers in size. However, the applicability of these theories to the colloidal behavior of true nanometer-sized particles is still questionable. For example, DLVO (Derjaguin-Landau-Verwey-Overbeek) theory models the interactions between colloidal particles and surfaces using only van der Waals force and electric double-layer interactions. DLVO is based on a continuum approach, neglecting solvent effects such as ion-solvent interactions, surface-solvent interactions, ion-ion correlation, and more [39]. When the particles are very close to each other or the particle size becomes small relatively close to the molecular size of the medium, the continuum theory of van der Waals and double-layer forces or the mean field theory should no longer be applied to describe the interaction between two surfaces [105]. In addition, the interaction between a particle and a polymer of similar nanosize must be considered in case of steric stabilization.

The surface force apparatus (SFA) and the atomic force microscope (AFM) have been useful tools for directly measuring the interaction forces between surfaces.

However, these techniques have several limits for studying forces of nanosize particles. For instance, SFA requires the molecularly smooth crossed cylindrical samples with a radius of the order of 1cm [89]. Even though AFM allows us to measure surface forces between any kind of surfaces, a direct force measurement using a conventional probe technique in AFM [61] is also limited to micron size colloidal particles due to the geometry and size of the tip. Although it is ideal to mount a single nano particle on the cantilever, handling and attaching it to the right position is empirically infeasible. In AFM, for instance, the attachable colloidal particle is normally a few tens of micrometers and the direct use of AFM tip has been employed in many studies have some controversy in measurement. For example, Cleveland measured oscillatory hydration potential on calcite ($CaCO_3$) and barite ($BaSO_4$) using thermal-mechanical noise of cantilever [106]. On the other hand, Kamiya utilized the Si_3N_4 AFM tip over one primary silica particle in water to study the effect of the particle size on the formation of hydration layer around the surface [107]. They observed with FT-IR and force measurement that no hydration force was found for nanoparticles with a diameter less than about 30 nm and suggested it could result from the different silanol structure on the surface of SiO_2 depending on the particle size.

Even though the nanometer size of radius of AFM tip may mimic the colloidal behavior of nanoparticle, the drawbacks such as difficulty of precise definition of the tip geometry and bluntness after several measurements cannot be neglected. In order to overcome this size limit for the colloidal probe technique, we suggest using a multiwalled carbon nanotube (MWNT) as a micron-length spacer and nanosized probe, so called nano colloidal probe. Using carbon nanotubes (CNT) as a STM or AFM probe has been

developed either by attaching it with glue [108] or growing it directly on the cantilever [109]. This small size probe is generally used for high-resolution imaging topography of a deep trenched sample. In addition, nanotubes have several advantages for investigating the interaction force of nanosized particles in AFM, that is, small diameter (2-20nm), hemispherical end structure, low surface roughness, and minimization of subsidiary effects from the AFM tip due to its high aspect ratio [108]. Recently, several researches have imaged the surfaces in a liquid system [108, 110], but direct force measurement and theories of interaction between nanosize particles are not well developed and only a few attempts have been made using this approach [111].

Work related to nanotubes in the AFM has employed the tapping mode, applying a small loading force in order to avoid the buckling of nanotube. However, one important feature in force measurement with the AFM is to determine zero separation. This needs linear compliance to convert a deflection-displacement curve to a force-separation curve, requiring a relatively high loading force. Thus, here will be demonstrated a modified colloidal probe technique with CNT for force measurement of nanosize particle and discussed how to determine zero distance when CNT is used as a probe.

Experimental

Materials

Multi-walled carbon nanotubes (MWNT) were extracted from the uncrushed carbon soot that was produced by arc-discharge method (Alfa Aesar, MA). This carbon soot was heat treated by thermogravimetric analysis (TGA) at 650°C in air flow to oxidize the carbonaceous materials such as amorphous carbon until the residual mass was less than 10 wt% of original mass of soot. By this method, many carbon nanotube bundles were exposed on the surface of the boule so that the next step could be

accomplished easily. No apparent defects such as an open cap or a partial oxidation of nanotubes were observed in SEM and TEM images. For the hydrophobic substrate, highly oriented pyrolytic graphite (HOPG, SPI supplies, PA) was used, which has a RMS roughness less than 0.05 nm within the area of $1\mu m^2$ and PECVD silica substrate was used as the hydrophilic substrate.

Preparation of Nanotube-Attached AFM Tip

For the nano probe preparation, a single MWNT bundle was mounted on the AFM using a method similar to that developed by H. Dai et al. [108]. Our method was slightly modified to make sure that the MWNT was stable on the end of the tip during force measurement in liquid. A schematic drawing of the mounting procedure of MWNT to the AFM tip is illustrated in Figure 5-1 and dark field optical microscope image is shown, too. MWNT bundles were aligned on a piece of SEM tape by barely touching the surface of the purified chunk of carbon nanotubes. The end of the AFM tip was then applied with a small amount of liquid state epoxy glue (UHU, Germany) and moved to the aligned MWNT bundles using two xyz micromanipulators (M-460A-XYZ, Newport, CA) in the inverted optical microscope (Carl Zeiss, Germany). After a long nanotube bundle was attached to the end, the AFM cantilever was heated to harden the epoxy glue at 200°C for 5 minutes and air-cooled to room temperature. Then, the AFM tip was weakly flushed with DI water, leaving a strongly attached MWNT bundle with a single protruding nanotube. It was confirmed by SEM that it was attached before and after the force measurement. The end of the single protruding MWNT is assumed to be closed and hemispherical because no electric current was applied for shortening.

(a)

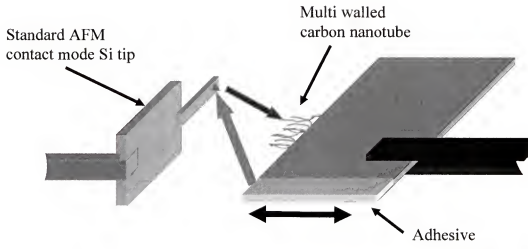

(b)

Figure 5-1. Preparation of the MWNT tip using a micromanipulator under the optical microscope. (a) Illustration showing the attachment of MWNT to the AFM tip. (b) A dark field optical image of the MWNT bundles aligned on the edge of the SEM tape and the AFM cantilever after attachment. Orange triangle is the tip of the cantilever.

Force Measurement

A commercial multimode AFM (Nanoscope III, Digital Instrument, CA) was utilized for force measurement using the contact mode Si tip (ESP, Digital Instrument, CA), which has a spring constant of 0.05 N/m and a 450 μm long cantilever. All measurements were conducted in a fused silica liquid cell where the AFM tip was located over the substrate. Working space between the tip and substrate was secured with silicone O-ring. Right before the force measurement, HOPG was freshly cleaved using double sticking tape and the MWNT probe was washed in ethanol and DI water. SiO_2 substrate was also cleaned with the same procedure as the previous chapter. All the accessories were ultrasonicated in the order of detergent, acetone, and ethanol for 30 minutes, respectively, rinsed with DI water, and blown with air for drying. The pH of solutions was adjusted with 1N HCl and 0.1 N NaOH in 0.01 M NaCl ionic strength. After the MWNT probe and substrate were loaded in the AFM, the solution was injected and allowed to equilibrate for 10 minutes. The force-separation plot was converted from the deflection signal-piezoscanner movement data, which was obtained by Z-scan rate of 500 nm/s.

Results and Discussion

Theoretical Calculation for the Effect of Tip Geometry

In theoretical calculations the standard AFM tip is very often considered as a sphere with a radius typically in the range of 5-100 nm [112, 113]. However, strictly speaking, the standard AFM tip is of pyramidal shape and has irregular apex, which may influence the direct force measurement between the tip and substrate. For simple calculation, AFM tip can be treated as a cone with an angle of 2θ attached with a half

sphere with radius R. The van der Waals force between the cone-shaped AFM tip and the flat substrate then can be described as [114]:

$$F(D)_{cone-plate} = -\frac{A}{6}\frac{D^2(R+D)\sin^2\theta + D^2 R\sin\theta + R^2(R+D)}{D^2(R+D)^2} \quad (5\text{-}1)$$

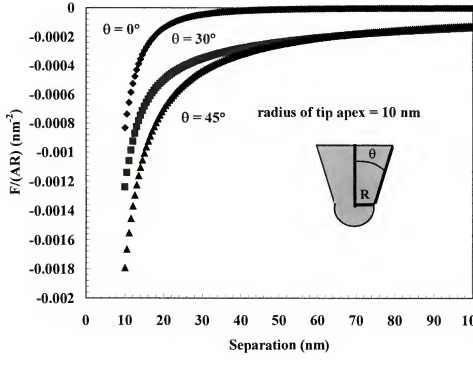

Figure 5-2. Calculated van der Waals interaction force between a cone shaped AFM tip and a flat plate depending on the angle θ.

Figure 5-2 shows how the side of the AFM tip will affect the total interaction force measurement depending on the angle between the vertical axis and side of the tip and the radius of curvature of the tip apex. As the angle increases, the resultant interaction force increases, suggesting the contribution from the side of the tip. The difference between the interaction forces depending on the angle is not trivial as the

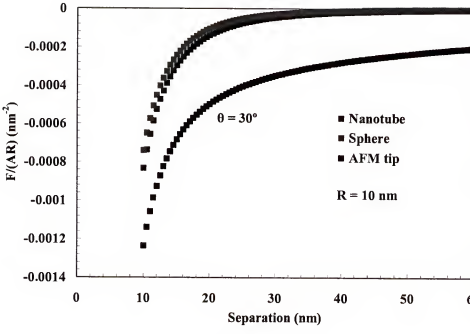

Figure 5-3. The calculated van der Waals interaction force between the colloidal probe and flat plate depending on the tip geometry.

radius of the tip apex decreases. However, when it comes to the nanotube probe, the angle between the wall and the tip apex can be considered as zero, minimizing the contribution from the side of the wall. The consequence is that the interaction force of nanotube tip is very similar to the force calculated with the nanospheres as shown in Figure 5-3.

The possible use of the nanotube as an alternative to the single nanoparticle to investigate the interaction force of nanoparticles can be validated with a theoretical calculation as shown in Figure 5-3. The calculated force with a conventional AFM tip is deviated much from the force of nano particle. On the other hand, a nanotube tip, which has a high aspect ratio, can well represent the interacting behaviors of the nano particles due to minimum effect from the side wall.

Figure 5-4 shows MWNT attached on the contact mode Si tip before and after measurement. As seen in the figure, MWNT is oriented vertically from the end of the tip. It should be mentioned that the shape of the AFM tip is important in achieving the vertical orientation of nanotube for force measurement. The tip angle of a conventional Si_3N_4 cantilever is too wide to obtain vertical orientation of MWNT. According to the manufacturer, the back side of this Si tip is about 10° steep, which helps in mounting the MWNT vertically. The length of the MWNT is usually about 1 μm and the diameter is about 20 nm.

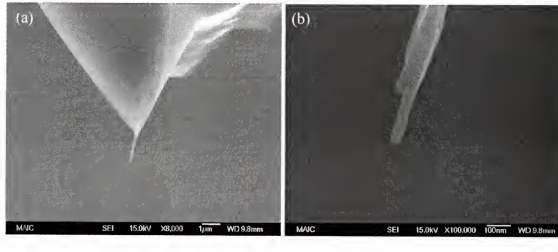

Figure 5-4. FESEM image of a MWNT bundle attached to the AFM tip. A shaded area on the tip is the melted epoxy resin holding the bundle of MWNT. (b) A high magnification FESEM image of the box in figure (a). One MWNT was protruded out of the bundle.

Surface force between Nanotube Tip and Substrate

The deflection signal obtained from the cantilever as the piezo scanner moves towards the AFM tip is shown in Fig. 5-5. It is necessary to analyze this data in detail prior to converting it to force-distance plots. The apparent deflection-displacement data

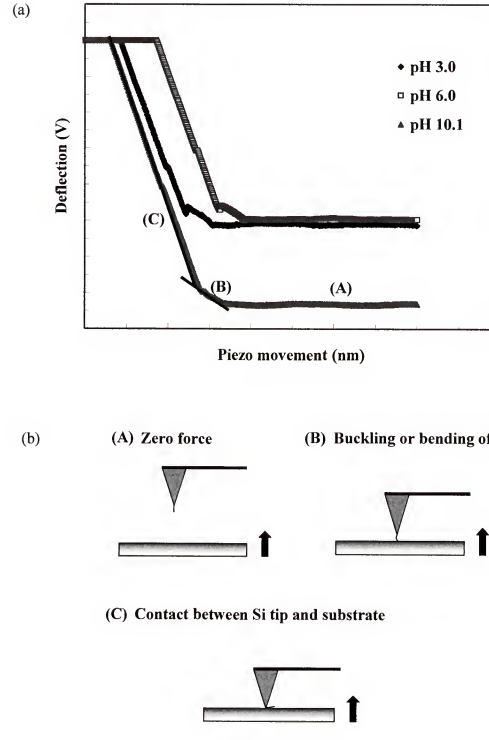

Figure 5-5. Deflection-displacement between highly oriented pyrolytic graphite (HOPG) and MWNT probe at different pH. (b) A schematic drawing of the nanoprobe and the substrate at regions (A), (B), and (C) during direct force measurement as shown in (a).

at different pHs were obtained with different Z-scan sizes and setting voltages. However, this difference is removed after force-distance conversion. In general, when substrate and MWNT probe are separated with a large distance, no deflection in the cantilever occurs. As separation distance is decreased, either an attractive or repulsive force is detected by the deflection of cantilever. However, two constant compliances were observed with MWNT probes as shown in Fig. 5-5. It is assumed that the two constant compliances result from the fact that two contacts exist, one of which is the contact between the MWNT and the substrate and the other is the contact between the Si tip and the substrate. In the region marked (A) in Fig. 5-5, no measurable force can be observed between the nanotube and the HOPG substrate. A force, if any, must appear right before the first contact between the nanotube and the substrate is made. After contact, a long MWNT would start to bend or buckle and slip on the surface (region (B) in Figure 5-5). This buckling force would absorb some fraction of energy that should be transferred to cantilever. Deformation mechanisms of nanotube tip during indentation were explored using molecular dynamics simulations [115] and similar buckling behavior is expected in our system. After the nanotube slipped on the sample surface, the second constant compliance was observed, which originated from the contact between Si tip and HOPG substrate (region (C) in Figure 5-5). The different slopes of the two constant compliances implicate the difference between the stiffness of the MWNT and the Si cantilever. The modulus of elasticity is reported to be about 1.2 TPa for MWNT whereas that of Si is known as about 47 GPa [116]. With a high modulus of elasticity, the nanotube has an excellent recovery without any plastic deformation after buckling. A schematic diagram of the behavior of MWNT probe is proposed in Figure 5-5 (b).

Other evidence that the second constant compliance comes from the contact between the Si tip and the substrate is the observation of a sudden jump of the tip onto the substrate between the two constant compliances, especially in low pH. This attractive behavior is expected to originate from the van der Waals force and/or the presumable hydrophobic force between Si tip and substrate. If the Si tip is naturally oxidized forming SiO_2, it is expected that the repulsive double layer force is very small (i.e. IEP of $SiO_2 \approx$ 2) and the attractive force is predominant at low pH. Even though HOPG is hydrophobic and SiO_2 is hydrophilic, hydrophobic force is expected with these dissimilar surfaces [117].

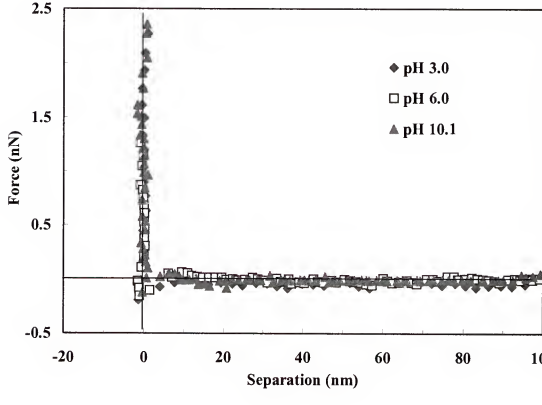

Figure 5-6. Force-separation profile between MWNT tip and HOPG substrate converted on the basis of the constant compliance, (B) in Figure 5-5.

Figure 5-6 represents the approaching force-separation curve converted on the basis of compliance (B) in Figure 5-5 (a), where separation between MWNT and substrate is determined to be zero. An attractive force was observed at a separation of about 5 nm irrespective of pH. It was concluded that the measured attractive force resulted from van der Waals attraction for the following reasons. First, there is no charge to be expected on the freshly cleaned graphite surface and MWNT. Therefore, electric double layer force can be excluded. The second possible forces that could be expected in such a system are hydrophobic forces. Hydrophobic forces typically have greater amplitude and longer interaction distances than van der Waals forces. According to the recent publications [118], hydrophobic forces occur when nanobubbles present on hydrophobic surfaces form a bridge. However, the here measured force was much smaller and appeared at a short distance. Therefore, it is concluded that no hydrophobic force contributes to the attraction due to the nanosize of MWNT.

Figure 5-7 and 5-8 represent the interaction force between MWNT and silica substrate as a function of ionic strength at pH 4 and 10. Unlikely to the interaction for the hydrophobic HOPG surface, attractive force occurred at low pH and repulsive force at high pH. This may be attributed to the EDL force between the silica surface and MWNT. According to the previous research on activated carbon [119], a heat treatment in H_2 or N_2 may lead to so-called L carbons, which have a low IEP. Even though the surface of the nanotube is relatively hydrophobic, there may be some defects by which carboxylic groups are formed on the surface during the heat treatment. Sun et al. measured the zeta potential of the pristine CNT and found the IEP to be about 5.8 [120].

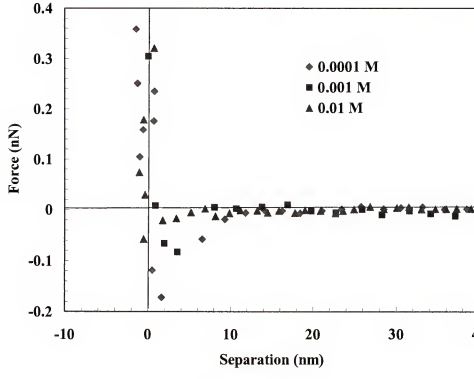

Figure 5-7. Interaction forces between MWNT tip and silica substrate as a function of ionic strength at pH 4.

If so, MWNT is positively charged at pH 4 and negatively charged at pH 10. Therefore, attractive force at low pH may be attributed to the attraction between the oppositely charged surfaces of silica and MWNT. Another indication of the electrostatic force between them is the dependence on the ionic strength. In other words, if the attractive force at low pH came from the vdW or hydrophobic force, it must be independent of the ionic strength. As seen in Figure 5-7, the attractive force decreased as the ionic strength increased due to the compression of the EDL subsequently reducing the electrostatic potential of the surfaces.

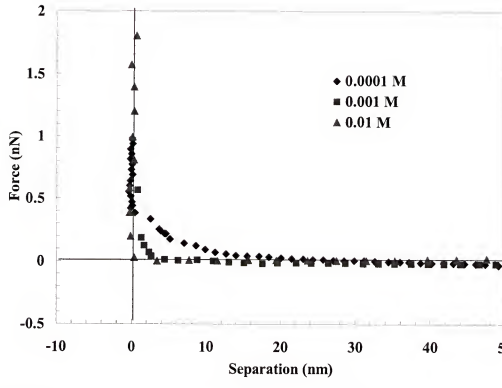

Figure 5-8. Interaction forces between MWNT tip and silica substrate as a function of ionic strength at pH 10

Summary

Despite the nanometer size of the AFM tip, the drawbacks of tip in the direct surface force measurement such as the irregular tip geometry and the contribution from the pyramidal shape of the tip cannot be neglected as seen in the theoretical calculation. The use of MWNT in the conventional liquid mode of AFM opens the possibility to directly measure the interaction force of true nanosize particles in various colloidal conditions. Determination of zero separation distance in the colloidal probe technique of AFM is essential in the direct force measurement between the MWNT probe and the sample. Two constant compliances are observed when the MWNT probe and the substrate contact each other due to the induced buckling of the nanotube. A force-

separation profile can be obtained on the basis of the first constant compliance between MWNT and substrate, for example, a small vdW attractive force was observed between MWNT and HOPG. This nanosize colloidal probe technique can allow us to measure directly the forces of nanosize particles, compare with theories, and answer the applicability of them beyond their original premise. Further, this nanotube probe can be utilized to understand the fundamentals of interaction between nanosize particles in the presence of polymer.

CHAPTER 6
EFFECT OF PARTICLE SIZE IN POLYMERIC FORCES

Introduction

Chapter 5 demonstrated the possibility of the carbon nanotube attached AFM tip as an alternative surface force measurement technique to conventional colloidal probe or the bare AFM tip for investigating the colloidal behavior of nanoparticles. In colloidal processing, the optimum amount of polymers or polyelectrolytes as dispersants must be chosen such that the maximum solids loading slurries are well stabilized without flocculation. A much lower or higher amount results in a flocculation, especially for high molecular weight polymers. A considerable experimental and theoretical knowledge of these behaviors has been established for particles on the micro or sub-micrometer range. However, understanding the behavior of nanoparticles with size of less than 100 nm is still limited. As the particle size decreases, the viscosity of nanoslurry increases and makes it difficult to achieve well-stabilized high solids loading slurries because the effective volume fraction increases. For example, Cesarano et al. [121] reported that dispersion of 62 vol% α-Al_2O_3 powders with size of 520 nm was achieved with polyacrylic acid (PAA). However, Rand et al. [122]reported that electrostatically dispersed δ-Al_2O_3 powders with average size of 10.7 nm showed the shear thinning behavior even with low solid contents (5-15 vol%). Nass et al. [123] also reported the non-Newtonian flow behavior of 11 vol% TiN powders with size of 30-40 nm using guanidine propionic acid (GPA).

The theories developed on the colloidal behavior of micronsized particles with polymers or polyelectrolytes have simply assumed particle surface to be flat because relative size difference between particles and polymer molecules are pretty large. However, as particle size decreases to a few nanometers range, this assumption must be reconsidered, i.e. the relative size of the polymer and colloidal particle may affect the conformation of the polymer. When polymer molecules interact with the nano particles, which have a relatively similar size to the polymer molecules, different conformation features are expected. According to molecular dynamics (MD) simulations [124] for the interaction of polyethylene oxide (PEO) with colloidal silica, polymers adopt a flat conformation on the surface when polymer molecules are much larger than the particles. In contrast, when the particle size increases, polymer adopts an extended conformation consisting of loops and tails. In addition to the relative size of polymer and particle, the surface chemical structure on nanoparticle itself might be changed due to large curvature of nanoparticle.

In this chapter, the surface force measurement between the MWNT probe and silica surfaces with the PEI addition will be compared with that of the micron-sized colloidal probe. Additionally, the effect of the free non-adsorbed macromolecules on the total interaction forces will be discussed depending on the size of interacting body, too.

Experimental

For micrometer-sized colloidal probe, a glassy carbon (Alfa Aeser, MA), which has a diameter of about 50 μm was attached with a low melting temperature resin (Epon R 1004, Shell Chemicals Co.) on the contact mode Si tip (ESP, Digital Instrument, CA). The spring constant of cantilever is 0.05 N/m, which is determined by thermal vibration

method. For nanometer-sized probe, MWNT attached tip was prepared by the method as described in the previous chapter. The substrate was a 2 μm thick PECVD SiO_2, whose RMS roughness was less than 0.3 nm. Different molecular weight PEIs (600, 1,800, 10,000, and 70,000 (30 w/v%)) were purchased from Alfa Aeser and diluted to the wanted concentration with ultrapure water. In order to see the effect of non-adsorbed macromolecules on the force measurement, silica colloidal probe with a diameter of about 45 μm was also prepared and colloidal silica (50 vol%, d_{50}=20 nm, Alfa Aeser) was diluted to 0.5, 2.5, and 5.0 vol%. 1 N HCl and 0.1 N NaOH were used for pH adjustment in 0.01 M NaCl ionic strength.

All the accessories, colloidal probe, and substrate were washed with the same procedure in the previous chapters and probe and substrate were cleaned again with ethanol and DI water prior to the experiment. All surface force measurements were performed in the liquid cell of the multimode Nanoscope III AFM. After the colloidal probe and substrate were loaded in the AFM, the PEI solution or colloidal silica suspension was injected and allowed to equilibrate for 15 minutes. The colloidal silica suspensions were ultrasonicated for 5 minutes right before the injection in order to break the possible coagulates during the storage. The force-separation profile was converted from the deflection signal and piezo scanner movement data, which was obtained by a Z-scan rate of 500 nm/s.

Results and Discussion

One example of the interaction force of MWNT tip in the presence of polyelectrolyte is represented in Figure 6-1. Force-separation plot was drawn as a function of added PEI 10,000 without replacing with the polymer-free bulk solution.

Without PEI, the recognizable interaction force was not observed in 0.01 M NaCl solution. It is similar to micronsized silica particles, because the layer thickness of PEI increases as the adsorption amount increases. The magnitude and range of the interaction force increased with increasing the concentration of PEI up to 1000 mg/L and showed maximum repulsive force of 0.25 nN and maximum interaction range of 10 nm above 1,000 mg/L. Good adsorption of PEI on the CNT in aqueous solution has been reported by Seeger et al. [125]. Sun et al. [120] observed the shift of IEP of pristine CNT from pH 5.8 to 10.8 with the adsorption of small amount of PEI as seen in zeta potential of the PEI adsorbed silica surfaces. As seen in the logarithmic plot in Figure 6-1, the electrostatic

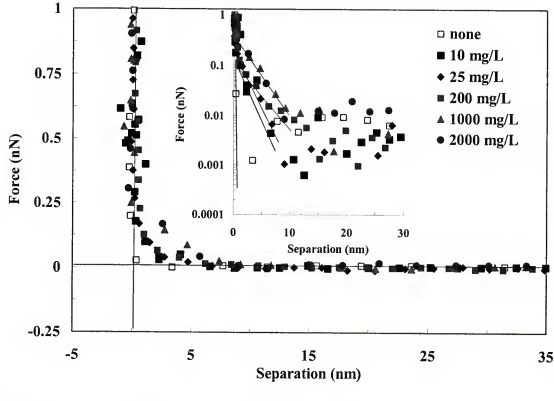

Figure 6-1. Interaction force between MWNT tip and silica substrate with a different concentration of PEI 10,000 in 0.01 M NaCl at pH 10. Solid lines in the inset are drawn for guidance.

interaction region was not observed due to high ionic strength and most interaction resulted from the polymeric layer adsorbed on the silica surface and nanotube. However, it must be noticed that the interaction range of polymer layers adsorbed on MWNT is smaller than that on the micron-sized silica particle, similarly observed with bare Si tip.

Effect of the Colloidal Probe Size

The interaction force with varying the concentration of PEI 70,000 for different sized colloidal probe was investigated. Figure 6-2 shows the normalized force-separation distance plot measured with a glassy carbon sphere with the different amount of the added polyelectrolyte. It was observed that the measured surface forces of micronsized colloidal probe were dependent on the polymer concentration. For the 0.06 wt% of PEI, incomplete coverage of the polymer layer seemed to take place considering the highest repulsive force occurred at a separation of 50 nm with 0.2 wt% of PEI. This repulsive barrier thickness is reasonable considering that the radius of gyration (R_g) for a linear PEI is 15.9 nm. This fits well to the 25 nm of the repulsive barrier thickness for the branched PEI. As the concentration of polymer was increased over 0.2 wt%, the interaction distance and repulsive forces were decreased. One feasible interpretation of this behavior may be the presence of free, non-adsorbed polymer. These free polymers may screen the interaction between the particles or the attractive forces may occur by the depletion due to the induced osmotic pressure when a large concentration of polymer is not adsorbed on the surface and the separation between surfaces is reduced to a critical distance. Additionally, it cannot be excluded at this point that entanglement of polymers may occur and thus a reduction of the repulsive forces with an increased polymer concentration. A large adhesion force up to separation of 100 nm (not shown here) was observed when the tip was retracted from the substrate at pH 10.

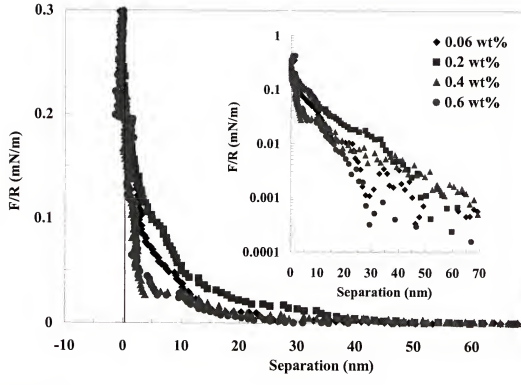

Figure 6-2. Force vs. separation plot between a glassy carbon and SiO_2 substrate in PEI 70,000 solution. Force dependence on the concentration of PEI was observed with the micronsized particle (pH 10, 0.01 M NaCl).

The force-separation distance profile with MWNT probe is shown in Figure 6-3. On the contrary to the micronsized particle, the same magnitudes of repulsive forces were observed even though the polymer concentration was varied. The interaction distance of a MWNT tip is of significantly shorter range than that of a micronsized glassy carbon tip. This behavior can be explained by the difference of probe size. The glassy carbon probe is much larger than the polymer allowing to interact with both tail and loop conformations of the adsorbed PEI and consequently measuring a far protruding layer. However, the nanosize MWNT is smaller than the dimension of the polymer chain and the polymer tails easily diffuse out of the tips range when the nanosize tip approaches.

Additionally, depletion effects may not play a significant role since the size of the nanotube tip is relatively small compared to the polymer molecules. Thus, the measured forces are independent of the concentration of PEI in the presence of nonadsorbed polymer. Depletion effect on the relative size of nonadsorbing particles for micronsized colloidal probe was recently studied with colloidal silica by Piech et al. [126]. They showed the decrease of depletion force with a large nonadsorbing particle.

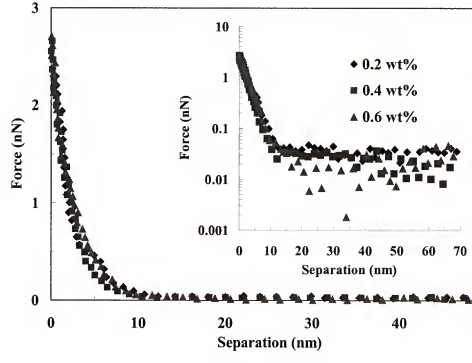

Figure 6-3. Force vs. separation plot between a MWNT probe and SiO_2 substrate. Measured forces were independent of the concentration of PEI (pH 10, 0.01 M NaCl).

For a comparison, the force-separation plot measured with a bare Si tip and silica substrate is shown in Figure 6-4. The interaction distance is smaller than the case of micronsized colloidal probe but similar to that measured with the MWNT tip because the radius of curvature of tip ending is about 10 nm. However, the forces which result from

the interaction between the side of the tip and substrate must be considered because the normal AFM tip is of a cone shape as explained in the previous chapter. Depletion effect was not observed with the bare silicon tip in the polymer concentration as high as 0.6 wt% to the contrary of the force measurement of glassy carbon sphere or MWNT probe. This may be from the different adsorption behavior of PEI on glassy carbon and Si i.e. glassy carbon has the less affinity of PEI on the surface.

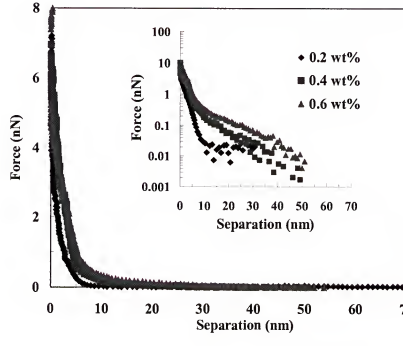

Figure 6-4. Force vs. separation plot between a bare Si tip and SiO_2 substrate (pH 10, 0.01 M NaCl)

Dependence of the steric forces of nanoparticle on the molecular weight of PEI was represented in Figure 6-5. All molecular weight PEI solution showed repulsive forces except for PEI 600, with which the attractive force was observed from a separation of 20 nm due to van der Waals force. The interaction range of steric force was 7 nm for PEI

1,800, 10 nm for PEI 10,000 and 70,000, respectively. Above this separation, data points were scattered because of the sensitivity of AFM.

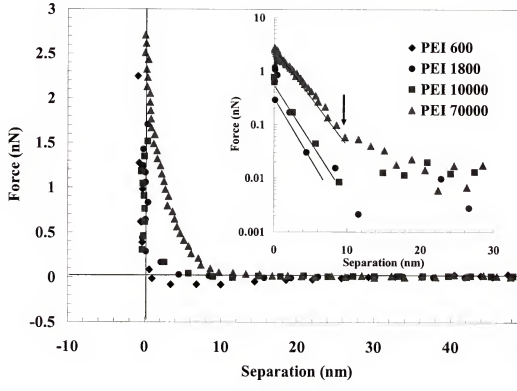

Figure 6-5. Interaction force between MWNT tip and silica substrate with 2000 mg/L PEI of different molecular weight in 0.01 M NaCl at pH 10.

Two important features of nanosized particles with PEI molecules can be addressed in this figure. One is the interaction range of steric force is smaller than that of micronsized particles. Braithwaite et al. [95] observed that the range of polymer induced repulsive force increases with the molecular weight of the adsorbed PEO. The thickness of adsorbed layer scales roughly with the molecular weight following the power law with the exponent 0.4. For comparison, whereas the steric repulsive forces for micronsized particles occurred at 20 nm and 50 nm of separation distance with PEI 10,000 and 70,000,

they took place at 10 nm of separation distance for the case of MWNT tip. Second interesting feature of the steric repulsive force with this small particle is that dependence of the interaction force on the separation distance is the same irrespective of the molecular weight. One possible explanation of these two features can be that nanoparticles adsorbed with polymers may interact only with the crowded PEI layers (i.e. loop-tail or loop-loop interaction) rather than loose PEI layers (i.e. tail-tail interaction). The other possible interpretation is that the flatter conformation of PEI may be built on nanoparticles due to the extremely large curvature.

Fitting the Interaction Force of MWNT Tip

There are several theories to describe the structure of polymer layers and the interaction force between polymer-coated surfaces. Most of them are based on either mean field approaches or scaling theories. Mean field approaches are the extended form of Flory-Huggins model of polymers in solution in that Gibbs free energy is calculated with the concentration gradients.

Based on the assumption of that the interaction force between two physically adsorbed polymer layers follows the inverse of power law of separation distance by mean field and scaling theory, the interaction force of MWNT tip was assumed to have a similar dependence on the separation distance as existing theories. Therefore, the fitting equation was assumed as

$$F = \frac{A}{H^n} \tag{6-1}$$

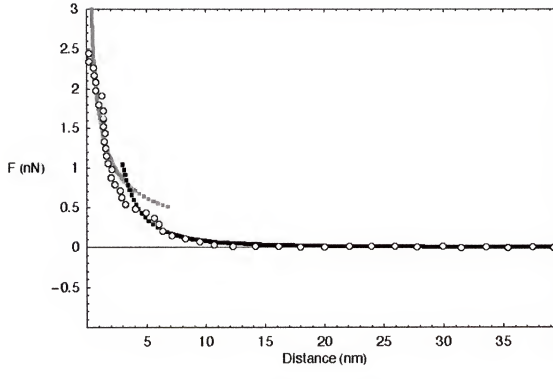

Figure 6-6. Force-separation profile of nanotube tip in presence of PEI 70,000 was fitted by the inverse power law. Open circle in figure denotes the force data measured.

Table 6-1. The fitting equation for the interaction force of MWNT tip at a short (< 2 nm) and long (> 5 nm) separation range

Concentration of PEI 70,000	Short distance	Long distance
0.2 wt%	$1.73\frac{1}{H^{0.56}}$	$155.6\frac{1}{H^{3.53}}$
0.4 wt%	$1.59\frac{1}{H^{0.27}}$	$44.8\frac{1}{H^{3.24}}$
0.6 wt%	$1.68\frac{1}{H^{0.19}}$	$48.0\frac{1}{H^{2.85}}$
Average	$\frac{1}{H^{0.34\pm0.2}}$	$\frac{1}{H^{3.20\pm0.34}}$

Recent simulation studies based on the scaling arguments identify the conformation transition of a polymer from a confined state to an escaped state when polymer chains are compressed by a finite-sized object [127, 128]. For example, the interaction force between a cylindrical tip with a flat bottom and a mushroom conformation of polymer can be expressed as

$$F_{confined} = 2c_1 \frac{Na^2}{H^3} \qquad \text{for confined chain} \qquad (6\text{-}2)$$

$$F_{escaped} = 2c_2 \frac{R_t}{H^2} \qquad \text{for escaped chain} \qquad (6\text{-}3)$$

where c_1 and c_2 are constants, N is the degree of polymerization, a is the monomer size, and R_t is the radius of the cylindrical tip. Therefore, the fitting of the force curve of the MWNT tip was made for two separation region. As shown in Figure 6-6, the fitting of interaction force of nanotube tip with 0.2 wt% PEI was conducted in two regions. Interaction forces of nanotube tip in other concentration of PEI 70,000 solution were also fitted by Equation 6-1 and the coefficient and the exponent were shown in Table 6-1. Above 5 nm (long range), the average force is inversely proportional to the third power of separation distance and it is inversely proportional to one third power of separation distance below 2 nm (short range). This is a significant difference with the micron sized particle, whose force is inversely proportional to the second power of separation distance in short range.

Effect of Non-adsorbed Free Polymer

In order to study the effect of the non-adsorbed polymer on the total interaction force, the force measurement can be performed in the solution with non-adsorbed macromolecules, followed by replacing with the pure bulk solution and comparing the

forces before and after washing. Figure 6-7 is the force-separation plot measured between silica sphere and silica substrate as a function of concentration of colloidal silica at pH 10, at which all interacting bodies are negatively charged and colloidal silica will not be adsorbed on the other surfaces due to electrostatic repulsion. As seen in the figures, the repulsive force was dramatically decreased with addition of the colloidal silica. The repulsive force decreased as the concentration of the colloidal silica increased. The same interaction force was recovered after washing with the pure electrolyte solution. Even though depletion attraction or screening the interacting surfaces may induce the decrease of repulsive force between silica surfaces, the apparent attractive forces were not observed, which may be due to the electrostatic repulsion.

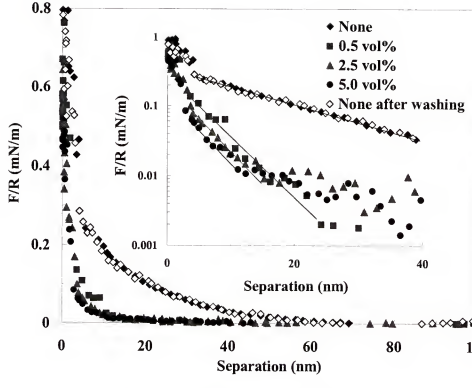

Figure 6-7. Interaction force between silica sphere and silica substrate at pH 10, 0.0001M as a function of concentration of colloidal silica.

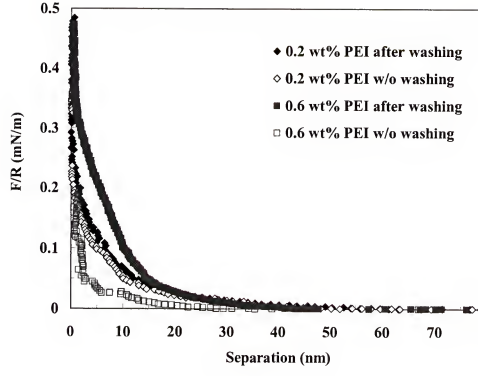

Figure 6-8. Force versus separation plot between a glassy carbon probe and SiO_2 substrate before and after washing out the non-adsorbed polymer in the solution.

Figure 6-8 shows the different force versus separation profile depending on the existence of the free polymers in the solution. First, 0.2 wt% or 0.6 wt% PEI solutions were injected into the liquid cell, which were left for 15 minutes for the PEI to adsorb on the surface of the sample. After measuring the force, the solution in the liquid cell was replaced with the bulk solutions, which were polymer-free and had same pH and ionic strength as the previously injected solution. For the 0.2 wt% solutions, both washed and non-washed solutions showed the same force-separation plot, which means most of polyelectrolytes were adsorbed on the surface. On the contrary, the much smaller repulsive forces were observed for the 0.6 wt% non-washed solution than the washed

solution. This indicates that a large amount of PEI, which was not adsorbed, induced the decrease of repulsive force between the PEI layers adsorbed on micrometer sized particles. The other possible reason of the decreased repulsive force may be the changes in conformation of the adsorbed polymers after the free polymers were removed by washing procedure.

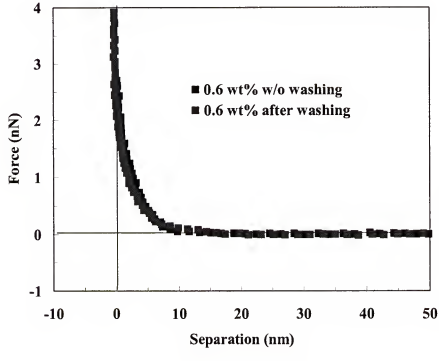

Figure 6-9. Force versus separation plot between a MWNT tip and SiO_2 substrate before and after washing out the non-adsorbed polymer in the solution.

The same washing procedure was carried out for the MWNT tip with 0.6 wt% PEI solution. Total interaction forces of MWNT tip were almost same before and after washing out non-adsorbed polymers as shown in Figure 6-9. Therefore, it can be concluded that as the particle size decreases to nanometer range, the effect of the non-

adsorbed polymers on the total surface force was not as significant as the micrometer sized particles due to similar size of particles and polymers.

Summary

The polymeric forces in the presence of PEI were discussed depending on the size of the probe. A nanosize MWNT probe clearly shows the independence of the concentration of polymer; whereas a micronsized glassy carbon sphere shows the larger polymeric interaction distance and the measured forces are functions of the concentration of polymer. The shorter interaction range and the same force dependence of the nano probe on the separation distance regardless of the molecular weight imply that nanoparticles may not interact with the loose polymer layer such as tails or the flatter polymer conformation may be formed on the surface of nanoparticles due to the large curvature. Another feature of the interaction between nanoparticles is that the polymeric force is inversely proportional to the one third power of the separation distance at a short interaction range while it is inversely proportional to the second power of separation distance. Decrease of the repulsive force due to the existence of the non-adsorbed free polymer was not observed in the MWNT probe and bare AFM tip because of the similar size as polymer molecules.

CHAPTER 7
CONCLUSION

Dispersion and flocculation of colloidal particles with polyelectrolytes is controlled by the electrostatic and polymeric interaction between them. In this study, first, adsorption behavior of cationic polyelectrolyte and its conformation on negatively charged solid surfaces were discussed by investigating the effect of pH, ionic strength, and molecular weight. As pH and ionic strength increases, the cationic polyelectrolyte PEI is of a folded or coiled structure subsequently occupying a smaller space at the solid/liquid interface. Because of the decrease of repulsion between the polymer segments and high nonelectrostatic affinity to the silica surfaces, the adsorbed amount increases with pH and ionic strength. High nonelectrostatic affinity at a high pH was also indicated by the increase of adsorption capacity with the molecular weight. The low adsorption amount and its independence of molecular weight at low pH suggested that adsorption mechanism is critically affected by the electrostatic repulsion between the polymer segments at low pH.

Stabilization mechanisms of colloidal particles could be anticipated with the adsorption isotherm and turbidity measurements. However, these experimental measurements are not sufficient to elucidate the polymer conformation on solid surface. For example, the low adsorption amount at a low pH can be made either by flat or standing conformation of the stretched polymer. The direct surface force measurement using the AFM colloidal probe technique could investigate the magnitude and the range of interactions between individual particles. Thin polymer layers were observed at a low

pH, which indicates that cationic polyelectrolytes are adsorbed on negatively charged surfaces in a flat conformation and swollen as ionic strength increases. These experimental combinations allow us to understand the fundamentals of stabilization of colloidal particles and to control precisely surface chemistry of particles for achieving high solids loading slurries.

The theoretical and experimental approaches to study surface forces in this manner have been dealing with the relatively large colloidal particles. By modifying the conventional colloidal probe technique with the carbon nanotube, we can extend the exploitable particle sizes down to nanometer range. This nano colloidal probe technique has merits over the bare AFM tip due to the great flexibility, small size and high aspect ratio of nanotube. Typical feature of the force measurement with the nanotube-attached AFM tip is that two constant compliance regions exist because of the buckling or bending of nanotube.

Clearly, when the particle size is close to that of polyelectrolyte, the interaction range of polymeric force of nanoparticle is smaller than that of micronsized particle. This suggests that the nanoparticle cannot interact with the whole segments of polymers, rather interact with the dense layer adsorbed on the surfaces such as loop structure. The polymeric force dependence on the separation distance was also found as particle size decreases. It was observed that non-adsorbed free polymers in solution do not have an influence on the surface forces of nanoparticles as much as on those of micronsized particles. These findings suggest that high molecular weight polymer may not be significantly effective to disperse the low solids loading nanoparticles because of similar interaction range irrespective of molecular weight. Rather, it may cause the increase of

viscosity of nanoparticle slurries due to the large effective volume of particles. In relatively high solids loading nanoparticle slurries, which induce the shorter separation distance between the particles, the higher molecular weight dispersant would be effective.

LIST OF REFERENCES

1. J. D. van der Waals, Over de Continuiteit van de Gas En Vloeistoftoestand (On the Continuity of the Gaseous and Liquid States). 1873, Leiden University: Netherlands.

2. A. Milling, P. Mulvaney, and I. Larson, J. Colloid Interf. Sci., **180** [2] 460 (1996).

3. S. Lee and W. M. Sigmund, J. Colloid Interf. Sci., **243** [2] 365 (2001).

4. W. H. Keesom, Communications Physical Laboratory, ed. H. Kamerlingh Onnes. 1912: Netherlands.

5. W. H. Keesom, Physics Z., **22** 129 (1921).

6. P. J. W. Debye, Physics Z., **21** 178 (1920).

7. F. London, Trans. Faraday Society, **33** 8 (1937).

8. H. C. Hamaker, Physica (Amsterdam), **4** 1058 (1937).

9. J. H. De Boer, Trans. Faraday Society, **32** 10 (1936).

10. I. E. Dzyaloshinskii, E. M. Lifshitz, and L. P. Pitaevskii, Adv. Phys., **10** [38] 165 (1961).

11. J. N. Israelachvili, Intermolecular and surface forces, 2nd ed. 1992, San Diego: Academic Press.

12. F. Wooten, Optical Properties of Solids, 1972, New York: Academic Press.

13. R. H. French, H. Mullejans, D. J. Jones, G. Duscher, R. M. Cannon, and M. Ruhle, Acta Mater., **46** [7] 2271 (1998).

14. R. H. French, J. Am. Ceram. Soc., **83** [9] 2117 (2000).

15. B. W. Ninham, J. Chem. Phys., **52** [9] 4578 (1970).

16. J. Mahanty and B. W. Ninham, Dispersion Forces, 1976, New York: Academic Press.

17. D. Tabor and Rh. Winterton, Proceedings of the Royal Society of London Series a-Mathematical and Physical Sciences, **312** [1511] 435 (1969).

18. H. D. Ackler, R. H. French, and Y. M. Chiang, J. Colloid Interf. Sci., **179** [2] 460 (1996).

19. R. H. French, R. M. Cannon, L. K. Denoyer, and Y. M. Chiang, Solid State Ionics, **75** 13 (1995).

20. H. B. G. Casimir and D. Polder, Physical Review, **73** [4] 360 (1948).

21. H. B. G. Casimir and D. Polder, Nature, **158** [4022] 787 (1946).

22. R. M. Pashley, J. Colloid Interf. Sci., **62** [2] 344 (1977).

23. W. B. Russel, D. A. Schowalter, and W. R. Saville, Colloidal Dispersions, 1989: Cambridge University Press.

24. B. V. Derjaguin, Kolloid Zeits, **69** 155 (1934).

25. R. J. Hunter, Foundations of Colloid Science, Vol. 1. 1989, Oxford: Clarendon Press.

26. G. A. Parks, Chem. Rev., **65** [2] 177 (1965).

27. G. Gouy, J. Phys. Radium., **9** 457 (1910).

28. D. L. Chapman, Phil. Mag., **25** 475 (1913).

29. O. Stern, Z. Electrochemistry, **30** 508 (1924).

30. D. C. Grahame, Chem. Rev., **41** 441 (1947).

31. P. Mulvaney, Nanoparticles and Nanostructured Films, ed. J.H. Fendler. 1998, Wiley-VCH: New York. 275.

32. M. V. Smoluchowski, Handbuch der Electrizitat und des Magnetismus, Vol. 2. 1921, Leipzeg: Brath.

33. E. Huckel, Physik. Z., **25** 204 (1924).

34. D. C. Henry, Proc. Roy. Soc., (London), **A133** 106 (1931).

35. R. Hogg, T. W. Healy, and D. W. Fuersten, Trans. Faraday Society, **62** [522P] 1638 (1966).

36. H. Ohshima, T. W. Healy, and L. R. White, J. Colloid Interf. Sci., **90** [1] 17 (1982).

37. B. V. Derjaguin and L. D. Landau, Acta Physicochim. USSR, **14** 633 (1941).

38. E. J. W. Verwey and T. G. Overbeek, Theory of Stability of Lyophobic Colloids, 1948, Amsterdam, Netherlands: Elsevier.

39. J. A. Greathouse and D. A. McQuarrie, J. Colloid Interf. Sci., **181** [1] 319 (1996).

40. R. G. Horn and J. N. Israelachvili, J. Chem. Phys., **75** [3] 1400 (1981).

41. W. M. Sigmund, N. S. Bell, and L. Bergstrom, J. Am. Ceram. Soc., **83** [7] 1557 (2000).

42. D. H. Napper, Polymeric Stabilisation of Colloidal Dispersions, 1983, London: Academic Press.

43. M. J. Garvey, T. F. Tadros, and B. Vincent, J. Colloid Interf. Sci., **49** [1] 57 (1974).

44. W. Kuhn, Kolloid Zeits, **68** 2 (1934).

45. G. J. Fleer, M. A. Cohen Stuart, J. H. M. H. Scheutjens, T. Cosgrove, and B. Vincent, Polymers at Interfaces, 1993: Chapman & Hall.

46. P. J. Flory, Statistical Mechanics of Chain Molecules, 1969, New York: J. Wiley.

47. P. G. Degennes, Adv. Colloid Interface Sci., **27** [3-4] 189 (1987).

48. S. T. Milner, T. A. Witten, and M. E. Cates, Europhys. Lett., **5** [5] 413 (1988).

49. S. T. Milner, T. A. Witten, and M. E. Cates, Macromolecules, **21** [8] 2610 (1988).

50. P. M. Claesson, H. K. Christenson, J. M. Berg, and R. D. Neuman, J. Colloid Interf. Sci., **172** [2] 415 (1995).

51. A. Dedinaite and P. M. Claesson, Langmuir, **16** [4] 1951 (2000).

52. M. L. Fielden and P. M. Claesson, J. Colloid Interf. Sci., **198** [2] 261 (1998).

53. M. Colic, M. L. Fisher, and G. V. Franks, Langmuir, **14** [21] 6107 (1998).

54. F. M. van der Kooij, A. P. Philipse, and J. K. G. Dhont, Langmuir, **16** [12] 5317 (2000).

55. M. Colic and D. W. Fuerstenau, Langmuir, **13** [25] 6644 (1997).

56. J. M. Cho and F. Dogan, J. Mater. Sci., **36** [10] 2397 (2001).

57. A. A. Zaman, M. Bjelopavlic, and B. M. Moudgil, J. Colloid Interf. Sci., **226** [2] 290 (2000).

58. J. N. Israelachvili and D. Tabor, Nature-Physical Science, **236** [68] 106 (1972).

59. D. C. Prieve and N. A. Frej, Langmuir, **6** [2] 396 (1990).

60. G. Binnig, C. F. Quate, and C. Gerber, Phys. Rev. Lett., **56** [9] 930 (1986).

61. W. A. Ducker, T. J. Senden, and R. M. Pashley, Nature, **353** [6341] 239 (1991).

62. D. Sarid, Scanning Force Microscopy, 1991: Oxford University Press.

63. J. E. Sader, I. Larson, P. Mulvaney, and L. R. White, Rev. Sci. Instrum., **66** [7] 3789 (1995).

64. C. T. Gibson, G. S. Watson, and S. Myhra, Nanotechnology, **7** [3] 259 (1996).

65. J. L. Hutter and J. Bechhoefer, Rev. Sci. Instrum., **64** [11] 3342 (1993).

66. J. L. Hutter and J. Bechhoefer, Rev. Sci. Instrum., **64** [7] 1868 (1993).

67. J. P. Cleveland, S. Manne, D. Bocek, and P. K. Hansma, Rev. Sci. Instrum., **64** [2] 403 (1993).

68. J. D. Holbery, V. L. Eden, M. Sarikaya, and R. M. Fisher, Rev. Sci. Instrum., **71** [10] 3769 (2000).

69. J. D. Holbery and V. L. Eden, J. Micromech. Microeng., **10** [1] 85 (2000).

70. V. A. Hackley, J. Am. Ceram. Soc., **80** [9] 2315 (1997).

71. T. F. Tadros, The Effects of Polymers on Dispersion Properties, 1981, London: Academic Press.

72. S. Baklouti, C. Pagnoux, T. Chartier, and J. F. Baumard, J. Eur. Ceram. Soc., **17** [12] 1387 (1997).

73. P. M. Claesson, O. E. H. Paulson, E. Blomberg, and N. L. Burns, Colloid Surf. A-Physicochem. Eng. Asp., **123** 341 (1997).

74. J. Sun, L. Gao, and J. Guo, J. Eur. Ceram. Soc., **19** [9] 1725 (1999).

75. T. Abraham, A. Kumpulainen, Z. Xu, M. Rutland, P. M. Claesson, and J. Masliyah, Langmuir, **17** [26] 8321 (2001).

76. Z. H. Pan, A. Campbell, and P. Somasundaran, Colloid Surf. A-Physicochem. Eng. Asp., **191** [1-2] 71 (2001).

77. G. M. Lindquist and R. A. Stratton, J. Colloid Interf. Sci., **55** [1] 45 (1976).

78. S. Akari, W. Schrepp, and D. Horn, Langmuir, **12** [4] 857 (1996).

79. T. Radeva and I. Petkanchin, J. Colloid Interf. Sci., **196** [1] 87 (1997).

80. R. Meszaros, L. Thompson, M. Bos, and P. de Groot, Langmuir, **18** [16] 6164 (2002).

81. X. W. Zhu, F. Q. Tang, T. S. Suzuki, and Y. Sakka, J. Am. Ceram. Soc., **86** [1] 189 (2003).

82. J. Wang and L. Gao, Nanostruct. Mater., **11** [4] 451 (1999).

83. J. Sun and L. Gao, J. Eur. Ceram. Soc., **21** [13] 2447 (2001).

84. Hostetle.Re and J. W. Swanson, J. Polym. Sci. Pol. Chem., **12** [1] 29 (1974).

85. M. R. Bohmer, O. A. Evers, and J. Scheutjens, Macromolecules, **23** [8] 2288 (1990).

86. O. A. Evers, G. J. Fleer, J. Scheutjens, and J. Lyklema, J. Colloid Interf. Sci., **111** [2] 446 (1986).

87. J. Scheutjens and G. J. Fleer, J. Phys. Chem., **83** [12] 1619 (1979).

88. H. G. M. Vandesteeg, M. A. C. Stuart, A. Dekeizer, and B. H. Bijsterbosch, Langmuir, **8** [10] 2538 (1992).

89. J. N. Israelachvili and G. E. Adams, Nature, **262** [5571] 773 (1976).

90. P. F. Luckham and S. Manimaaran, Adv. Colloid Interface Sci., **73** 1 (1997).

91. J. N. Israelachvili, M. Tirrell, J. Klein, and Y. Almog, Macromolecules, **17** [2] 204 (1984).

92. J. L. Parker, Prog. Surf. Sci., **47** [3] 205 (1994).

93. H. G. Pedersen and L. Bergstrom, J. Am. Ceram. Soc., **82** [5] 1137 (1999).

94. E. Laarz, A. Meurk, J. A. Yanez, and L. Bergstrom, J. Am. Ceram. Soc., **84** [8] 1675 (2001).

95. G. J. C. Braithwaite and P. F. Luckham, J. Chem. Soc. Faraday Trans., **93** [7] 1409 (1997).

96. E. Poptoshev and P. M. Claesson, Langmuir, **18** [7] 2590 (2002).

97. A. Janshoff, M. Neitzert, Y. Oberdorfer, and H. Fuchs, Angew. Chem.-Int. Edit., **39** [18] 3213 (2000).

98. Y. I. Rabinovich, B. V. Derjaguin, and N. V. Churaev, Adv. Colloid Interface Sci., **16** [7] 63 (1982).

99. A. Grabbe and R. G. Horn, J. Colloid Interf. Sci., **157** [2] 375 (1993).

100. A. Grabbe, T. A. Michalske, and W. L. Smith, J. Phys. Chem., **99** [13] 4648 (1995).

101. V. V. Yaminsky, B. W. Ninham, and R. M. Pashley, Langmuir, **14** [12] 3223 (1998).

102. G. B. Alexander, W. M. Heston, and R. K. Iler, J. Phys. Chem., **58** [6] 453 (1954).

103. I. U. Vakarelski, K. Ishimura, and K. Higashitani, J. Colloid Interf. Sci., **227** [1] 111 (2000).

104. A. Dietrich and A. Neubrand, J. Am. Ceram. Soc., **84** [4] 806 (2001).

105. P. Mulvaney, J. M. Perera, S. Biggs, F. Grieser, and G. W. Stevens, J. Colloid Interf. Sci., **183** [2] 614 (1996).

106. J. P. Cleveland, T. E. Schaffer, and P. K. Hansma, Phys. Rev. B, **52** [12] R8692 (1995).

107. H. Kamiya, M. Mitsui, H. Takano, and S. Miyazawa, J. Am. Ceram. Soc., **83** [2] 287 (2000).

108. H. J. Dai, J. H. Hafner, A. G. Rinzler, D. T. Colbert, and R. E. Smalley, Nature, **384** [6605] 147 (1996).

109. C. L. Cheung, J. H. Hafner, T. W. Odom, K. Kim, and C. M. Lieber, Appl. Phys. Lett., **76** [21] 3136 (2000).

110. K. Moloni, M. R. Buss, and R. P. Andres, Ultramicroscopy, **80** [4] 237 (1999).

111. S. P. Jarvis, T. Uchihashi, T. Ishida, H. Tokumoto, and Y. Nakayama, J. Phys. Chem. B, **104** [26] 6091 (2000).

112. C. Argento and R. H. French, J. Appl. Phys., **80** [11] 6081 (1996).

113. C. J. Drummond and T. J. Senden, Colloid Surf. A-Physicochem. Eng. Asp., **87** [3] 217 (1994).

114. H. G. Pedersen, Particle Interactions: An AFM Study of Colloidal Systems, in Department of Chemistry, 1998, Technical University of Denmark.

115. A. Garg, J. Han, and S. B. Sinnott, Phys. Rev. Lett., **81** [11] 2260 (1998).

116. E. W. Wong, P. E. Sheehan, and C. M. Lieber, Science, **277** [5334] 1971 (1997).

117. Y. H. Tsao, D. F. Evans, and H. Wennerstrom, Science, **262** [5133] 547 (1993).

118. N. Ishida, T. Inoue, N. Miyahara, and K. Higashitani, Langmuir, **16** [16] 6377 (2000).

119. J. A. Menendez, J. Phillips, B. Xia, and L. R. Radovic, Langmuir, **12** [18] 4404 (1996).

120. J. Sun, L. Gao, and W. Li, Chem. Mater., **14** [12] 5169 (2002).

121. J. Cesarano and I. A. Aksay, J. Am. Ceram. Soc., **71** [12] 1062 (1988).

122. B. Rand and R. Fries, Ceramic Transactions: Vol. Science, Technology, and Coomercialization of Powder Synthesis and Shape Forming, ed. J.J. Kingsley, C.H. Shilling, and J. Adair.. 1996, Westerville, OH: American Ceramic Society. 165.

123. R. Naas, S. Albayrak, M. Aslan, and M. Schmidt, Ceramic Transactions: Vol. Ceramic Processing Science and Technology, ed. H. Hausner, G.L. Messing, and S.-I. Hirano. 1994, Westerville, OH: American Ceramic Society. 591.

124. T. Cosgrove, P. C. Griffiths, and P. M. Lloyd, Langmuir, **11** [5] 1457 (1995).

125. T. Seeger, P. Redlich, N. Grobert, M. Terrones, D. R. M. Walton, H. W. Kroto, and M. Ruhle, Chem. Phys. Lett., **339** [1-2] 41 (2001).

126. M. Piech, P. Weronski, X. Xu, and J. Y. Walz, J. Colloid Interf. Sci., **247** [2] 327 (2002).

127. M. C. Guffond, D. R. M. Williams, and E. M. Sevick, Langmuir, **13** [21] 5691 (1997).

128. G. Subramanian, D. R. M. Williams, and P. A. Pincus, Macromolecules, **29** [11] 4045 (1996).

BIOGRAPHICAL SKETCH

Jeong-Min Cho was born in Yeosu, Korea on October 3, 1971. He was raised there with his sister and brother until he graduated from Yeosu High School, where he was valedictorian of the class of 1989. He entered Seoul National University, Seoul, Korea, in the Department of Petroleum and Mineral Engineering in 1991. After his sophomore year, he served in the Korean Air Force in Seongnam, Korea for one-and-a-half years. Then he returned to school, earning a Bachelor of Science degree in Fall 1996. He then continued his education at the University of Washington (Seattle) in the Department of Materials Science and Engineering, earning a Master of Science degree in Summer 1999. He transferred to the University of Florida (Gainesville) in pursuit of a Doctor of Philosophy degree in the Department of Materials Science and Engineering. He earned this degree in Fall 2003 specializing in ceramics science and engineering. He plans to return to his country, to join Samsung Electro-Mechanics Corporation in Suwon, Korea.

I certify that I have read this study and that in my opinion it conforms to acceptable standards of scholarly presentation and is fully adequate, in scope and quality, as a dissertation for the degree of Doctor of Philosophy.

Wolfgang M. Sigmund, Chair
Associate Professor of Materials Science and Engineering

I certify that I have read this study and that in my opinion it conforms to acceptable standards of scholarly presentation and is fully adequate, in scope and quality, as a dissertation for the degree of Doctor of Philosophy.

Brij M. Moudgil
Distinguished Professor of Materials Science and Engineering

I certify that I have read this study and that in my opinion it conforms to acceptable standards of scholarly presentation and is fully adequate, in scope and quality, as a dissertation for the degree of Doctor of Philosophy.

Susan B. Sinnott
Associate Professor of Materials Science and Engineering

I certify that I have read this study and that in my opinion it conforms to acceptable standards of scholarly presentation and is fully adequate, in scope and quality, as a dissertation for the degree of Doctor of Philosophy.

Laurie B. Gower
Associate Professor of Materials Science and Engineering

I certify that I have read this study and that in my opinion it conforms to acceptable standards of scholarly presentation and is fully adequate, in scope and quality, as a dissertation for the degree of Doctor of Philosophy.

Dinesh O. Shah
Professor of Chemical Engineering

This dissertation was submitted to the Graduate Faculty of the College of Engineering and to the Graduate School and was accepted as partial fulfillment of the requirements for the degree of Doctor of Philosophy.

December 2003

Pramod Khargonekar
Dean, College of Engineering

Winfred M. Phillips
Dean, Graduate School